NASA TECHNICAL NOTE

NASA TN D-7485

NASA TN D-7485

TRANSPORT ANALYSIS OF MEASURED NEUTRON LEAKAGE SPECTRA FROM SPHERES AS TESTS OF EVALUATED HIGH-ENERGY CROSS SECTIONS

by Donald Bogart, Donald F. Shook, and Daniel Fieno

Lewis Research Center
Cleveland, Ohio 44135

NATIONAL AERONAUTICS AND SPACE ADMINISTRATION • WASHINGTON, D. C. • NOVEMBER 1973

1. Report No.	2. Government Accession No.	3. Recipient's Catalog No.
NASA TN D-7485		

4. Title and Subtitle	5. Report Date
TRANSPORT ANALYSIS OF MEASURED NEUTRON LEAKAGE SPECTRA FROM SPHERES AS TESTS OF EVALUATED HIGH-ENERGY CROSS SECTIONS	November 1973
	6. Performing Organization Code

7. Author(s)	8. Performing Organization Report No.
Donald Bogart, Donald F. Shook, and Daniel Fieno	E-7327
	10. Work Unit No. 503-10
9. Performing Organization Name and Address Lewis Research Center National Aeronautics and Space Administration Cleveland, Ohio 44135	11. Contract or Grant No.
	13. Type of Report and Period Covered Technical Note
12. Sponsoring Agency Name and Address National Aeronautics and Space Administration Washington, D.C. 20546	14. Sponsoring Agency Code

15. Supplementary Notes

16. Abstract

Integral tests of evaluated ENDF/B high-energy cross sections have been made by comparing measured and calculated neutron leakage flux spectra from spheres of various materials. An Am-Be (α,n) source was used to provide fast neutrons at the center of the test spheres of Be, CH_2, Pb, Nb, Mo, Ta, and W. The absolute leakage flux spectra were measured in the energy range 0.5 to 12 MeV using a calibrated NE213 liquid scintillator neutron spectrometer. Absolute calculations of the spectra were made using version III ENDF/B cross sections and an S_n discrete ordinates multigroup transport code. Generally excellent agreement was obtained for Be, CH_2, Pb, and Mo, and good agreement was observed for Nb although discrepancies were observed for some energy ranges. Poor comparative results, obtained for Ta and W, are attributed to unsatisfactory nonelastic cross sections. The experimental sphere leakage flux spectra are tabulated and serve as possible benchmarks for these elements against which reevaluated cross sections may be tested.

17. Key Words (Suggested by Author(s))	18. Distribution Statement
Sphere leakage spectra; Scintillator measurements; Neutron flux spectra; Nuclear reactors; Neutron cross sections	Unclassified - unlimited

19. Security Classif. (of this report)	20. Security Classif. (of this page)	21. No. of Pages	22. Price*
Unclassified	Unclassified	39	Domestic, $3.00 Foreign, $5.50

* For sale by the National Technical Information Service, Springfield, Virginia 22151

TRANSPORT ANALYSIS OF MEASURED NEUTRON LEAKAGE SPECTRA FROM SPHERES AS TESTS OF EVALUATED HIGH-ENERGY CROSS SECTIONS

by Donald Bogart, Donald F. Shook, and Daniel Fieno

Lewis Research Center

SUMMARY

Integral tests of evaluated ENDF/B high-energy cross sections have been made by comparing measured and calculated neutron leakage flux spectra from spheres of various materials. An americium-beryllium (Am-Be (α, n)) source was used to provide fast neutrons at the center of the test spheres of beryllium (Be), polyethylene (CH_2), lead (Pb), niobium (Nb), molybdenum (Mo), tantalum (Ta), and tungsten (W). The absolute leakage flux spectra were measured in the energy range 0.5 to 12 MeV using a calibrated NE213 liquid scintillator neutron spectrometer. Absolute calculations of the spectra were made using version III ENDF/B cross sections and an S_n discrete ordinates multigroup transport code.

Generally excellent agreement was obtained for Be, CH_2, Pb, and Mo, and good agreement was observed for Nb, although discrepancies were observed for some energy ranges. Poor comparative results, obtained for Ta and W, are attributed to unsatisfactory nonelastic cross sections. The experimental sphere leakage flux spectra are tabulated and serve as possible benchmarks for these elements against which reevaluated cross sections may be tested.

INTRODUCTION

An effort continues to develop improved neutron cross section libraries (ref. 1). The absolute precision required by reactor and shield analysts is dependent on the sensitivity of performance criteria to uncertainties in cross sections. Because of the spectral and importance variations in reactors, these sensitivities are difficult to specify in general terms and existing problems are recognized (ref. 2). Except for isolated isotopes such as hydrogen (H) or carbon (C), which qualify as absolute standards for total cross section, and a few isotopes such as lithium-6 (^{6}Li), boron-10 (^{10}B), gold-197 (^{197}Au),

and uranium-238 (^{238}U), which ultimately may qualify as secondary standards for capture cross sections, an atmosphere of controversy and uncertainty still exists (refs. 3 to 6).

Cross sections for most of the important elements are gradually being remeasured and reevaluated. For example, the state of the art and the dilemmas facing the cross section evaluator are well documented by Davey (ref. 7) for the case of ^{238}U fast neutron data. In addition, a discussion by Orphan (ref. 8) has reviewed cross sections for reactors and shields and has drawn attention to recent developments in techniques for measuring elastic and inelastic scattering cross sections. For example, improved fast neutron time-of-flight LINAC based systems have permitted measurements for many elements up to ~9 MeV (ref. 9). Experimental resolution is sufficient to determine inelastic scattering peaks for lower energy isolated levels for middle weight elements and to indicate considerable structure for the unresolved higher energy levels. These measurements raise questions about the adequacy of representing inelastic cross section as smooth average curves in ENDF/B files. In addition, for some elements, inelastic down scattering is represented crudely by the evaporation model with spectra defined by an energy dependent nuclear temperature.

The situation is perhaps analogous to that for capture cross sections in the kilo-electron-volt region where the resolution of the best time-of-flight systems with linear accelerators is inadequate to define isolated level structure above a few keV. A knowledge of the structure is required for fast spectrum reactors and shields. The pitfall of assuming that the capture cross sections are smooth is illustrated by recent calculations of sphere transmission data (refs. 10 to 13) which account for resonance structure of the unresolved cross sections. These Monte Carlo calculations used resonance parameters selected from merged and separated spin statistics and have shown relatively large errors in the absolute cross sections at 24 keV obtained from a smooth cross section approximation.

For neutron flux calculations, the use of modern transport methods and references to programs coded for digital computers using the discrete ordinates and the Monte Carlo methods have been summarized by Maienschein et al. (ref. 14). What are needed by reactor and shield analysts are nuclear data files of sufficient precision such that designers have a high degree of confidence in applying the increasingly available neutron and gamma-ray multigroup transport computer codes. The credibility of the design methods using these codes that employ ENDF cross section libraries lies in the degree of correlation obtained between results of integral experiments and their analyses. Integral experiments for both critical assemblies (ref. 15) and so-called benchmark shield configurations have been performed (ref. 16). Benchmark experiments consist of well documented integral experiments with various media and ideally should be simple in geometry and homogeneous in composition. They should be designed to permit measurement of absolute neutron energy spectra and angular fluxes so as to facilitate the checking of

transport calculational methods and the completeness and precision of neutron cross section sets used. A recent review by Straker (ref. 17) discusses the integral experiments that have been performed and presents a background on the evolution of benchmark problems.

It has been argued that accurate prediction of measured integral quantities such as critical masses, material reactivities, and spectral detector indices have inherent limitations and may contain compensating effects that mask potentially large uncertainties in reactor spectra and/or cross sections. An example of the limitations of measuring spectral indices in spherical samples within a fast reactor assembly as commentaries on nonelastic scattering cross sections has been presented by Davey and Amundson (ref. 18). Another complication is the presence of several elements in addition to fissionable materials in critical assemblies that makes it difficult to attribute discrepancies to specific isotopes. Therefore, alternative integral experiments have been sought that have elemental compositions.

It is clear that experiments that are projected as definitive tests of the precision of ENDF/B cross sections should provide differential data so that comparison with calculations can serve as commentary on the validity of cross sections over particular energy ranges. In this connection the organic liquid scintillator measurements of spectra for uncollided fission neutrons transmitted through thick samples of material (refs. 19 and 20) was a pioneering step in obtaining differential data to test total cross sections. Here, comparison of measured and calculated transmission spectra from ~ 0.8 to 12 MeV for many materials served primarily as tests of minima in neutron total cross sections.

Another method for obtaining differential data from idealized experiments employs time-of-flight techniques to measure fast neutron angular flux spectra at different positions in simple homogeneous assemblies. Representative of these experiments is the work of Profio, Cerbone, and Huffman (ref. 21) with relatively thick spheres of paraffin and lithium hydride and centrally located photofission sources. Since the sphere is a one-dimensional medium and, if homogeneous and composed of one element, it is the ideal integral experiment. Neutron energy spectra and angular fluxes are measured by extracting a collimated beam from various positions and at various angles in the media. Interpretation of the measured angular flux spectra by multigroup transport calculations requires (1) a careful absolute experimental method for normalizing the calculated and experimental data and (2) a higher order angular quadrature than ordinarily employed to calculate scalar flux spectra. The experience of Profio, Cerbone, and Huffman (ref. 21) in calculating the measured anisotropic distribution of angular flux, particularly in the forward direction, was that it would be necessary to use a very fine angular mesh that would require considerable computer storage. The alternative is to use asymmetrical quadrature sets to calculate highly forward directed neutron angular fluxes as proposed

by Cerbone and Lathrop (ref. 22). However, the angular quadrature used in many reactor and shield designs is a compromise between angular resolution and computer storage requirements.

The need for clean, homogeneous integral experiments against which multigroup transport calculations may be tested is apparent. In the present study, an americium-beryllium (Am-Be) neutron source was employed at the center of various spherical media. Sphere leakage spectra were measured using an NE213 organic liquid scintillator neutron spectrometer in the energy range 0.5 to 12 MeV. Materials studied were beryllium (Be), polyethylene (CH_2), lead (Pb), niobium (Nb), molybdenum (Mo), tantalum (Ta), and tungsten (W). Preliminary portions of this work were reported earlier (refs. 23 and 24).

It is suggested that these sphere experiments can serve as benchmark data for the measured energy range. Future work should be encouraged using other spheres and californium-252 (^{252}Cf) fission sources and augmenting the energy range of measurement by employing proportional counters for the keV energy range.

EXPERIMENT

A radioactive Am-Be (α,n) source was used in conjunction with a fast neutron spectrometer to measure neutron spectra in the energy range from 0.5 to 12 MeV. The (α,n) source was placed at the center of spheres of various test materials, and the leakage flux spectra measured at a distance of 200 centimeters from the source to the spectrometer. The experimental arrangement is shown in figure 1 where both the source and spectrometer are located 160 centimeters above the floor. Background contributions due to neutrons scattered into the spectrometer from the walls of the room and from the supporting structures were measured using a paraffin shadow cone. Background corrections to the measurements were negligible at the higher neutron energies but increased to 30 percent at 500 keV.

Test Material Spheres

The spheres used are fairly thick, being generally of the order of several mean free paths at 4 MeV so that a large percentage of the source neutrons have interacted with the sphere before arriving at the spectrometer. Materials studied were Be, CH_2, Pb, Nb, Mo, Ta, and W. For the heavier materials little energy transfer occurs by elastic processes and for Be the (n, 2n) processes are important. The experiments are, therefore, primarily sensitive to the nonelastic cross sections and in particular to the spectra of the inelastically scattered neutrons. Since a large percentage of the neutrons

from a Be (α, n) source lie in the energy range 2 to 8 MeV, the experiment is particularly sensitive to inelastic reactions occurring in this energy range.

Each test sphere employed contained a central cavity 6.15 centimeters in diameter to accommodate the Am-Be source. The metallic spheres used were machined or cast of high purity metal with the exception of Nb that contains 0.95 percent by weight of Zr. The spheres containing Mo and W were fabricated of 0.050-centimeter steel sheet and filled with Mo powder or fine W balls. In order to study a thick W case, a second, larger W sphere was composed of fine W balls in a 0.48-centimeter steel container. The composition and sizes of the spheres are given in table I. For the case of Pb the isotopic composition can vary, depending on the geographical location of the source of the Pb. The Pb used in the sphere has a measured isotopic composition close to that of natural Pb; the measured abundances are 51.37 percent ^{208}Pb, 20.50 percent ^{207}Pb, 26.83 percent ^{206}Pb, and 1.29 percent ^{204}Pb. For purposes of intercomparison with a material of well known cross sections, a CH_2 sphere made from high density polyethylene was included.

Neutron Spectrometer

Neutron flux spectra from the Am-Be source and the various spheres were measured using a 5- by 5-centimeter cylindrical NE213 liquid scintillator proton recoil spectrometer. The virgin (α, n) spectrum used as input in the transport calculations was obtained from measurements using a smaller scintillator. The large liquid scintillator has the advantages of high sensitivity and well calibrated neutron response functions (ref. 25) while the smaller one has better resolution. Although the resolution of scintillation spectrometers is poor compared with that of time-of-flight measurements, it has been measured and is comparable with the energy widths of the neutron groups used in the multigroup transport calculations. A direct and more convenient comparison of the experimental spectra with multigroup transport calculations is possible, provided that the spectrometer resolution function is folded into the multigroup analytical results. This procedure is discussed in the next section of this report. A curve of the energy resolution of the 5- by 5-centimeter NE213 liquid scintillator is presented by Straker (ref. 20) and indicates the resolution to be 10 percent at 11 MeV and to become progressively poorer to 20 percent at 3 MeV and 35 percent at 1 MeV. For a cylindrical scintillator as large as the 5- by 5-centimeter size, care must be exercised in determining the neutron spectra from the measured proton recoil spectra due to additional contributions caused by multiple scattering and carbon interactions in the scintillator. These effects are reviewed in detail by Shook and Pierce (ref. 26).

In the present experiments the measured proton recoil spectra were reduced using the calibrations of Verbinski, et al. (ref. 25) and the unfolding code, FERDOR (ref. 27)

for the case of the detector in a parallel beam of neutrons incident on the curved surface. The present sphere measurements are in an essentially parallel beam geometry because of the large separation distance between the source and detector so that the response functions generated for this mode of operation are directly applicable. To assure that small differences in scintillator size or spectrometer resolution do not cause a significantly different response matrix, monoenergetic neutron spectra were measured at 2.8 and 14.7 MeV; detailed comparison indicated that response functions agreed satisfactorily with the response functions of reference 25.

Pulse shape analysis and two-parameter data acquisition were used to discriminate against γ-ray pulses. A block diagram of the spectrometer is shown in figure 2 along with the photomultiplier tube base circuit. A linear pulse is taken from the ninth dynode of the photomultiplier tube, amplified and sent to one side of the analyzer. A pulse whose amplitude depends strongly on the shape of the linear pulse is taken from the 12th dynode. Commercially available amplifiers and analyzer are used. The Owens type pulse shape circuit utilizing space-charge saturation is built into the dynode chain of the RCA 8575 tube. The two diodes shown in the circuit eliminate the unwanted large negative part of the pulse obtained from this type of circuit (ref. 28). With 2000 volts across the tube dynode chain, it is possible to separate neutron and γ-ray interactions down to 20-keV electron energy, which corresponds to a proton energy of 200 keV. This separation has been achieved in a 10-to-1 ratio of gamma-to-neutron field.

The spectrometer has been calibrated using a sodium-22 (^{22}Na) γ-ray source. A calibration curve is shown in figure 3. The calibration energy of 1.12-MeV electron energy corresponds to the half height of the Compton edge. Additional information on the spectrometer and data reduction methods used here is described by Shook and Pierce (ref. 26). They also measured neutron spectra for a small polonium-beryllium (Po-Be) neutron source with three organic liquid scintillators, two smaller in size than the 5- by 5-centimeter detector, and compared results with the spectra measured by the calibrated 5- by 5-centimeter NE213 detector. The spectra for the smaller cylindrical detectors were obtained by differentiation of the proton recoil pulse height spectra. The approximations involved in the differentiation analysis were indicated to have small effects on the precision of the neutron spectra measured with the smaller scintillators but did introduce significant error for the larger 5- by 5-centimeter detector. The advantage of using the smallest cylindrical scintillator, which measured 1.2- by 1.3-centimeter, is that its resolution is considerably greater than that of the 5- by 5-centimeter detector. For example, the measurements reported by Shook (ref. 26) showed the smaller detector to have a resolution (width at half maximum) of 8.6 percent at a monoenergetic neutron energy of 2.84 MeV compared with a resolution of 20 percent for the 5- by 5-centimeter detector at this energy cited by Straker (ref. 20). Similar results were obtained for proton recoil data corresponding to a neutron energy of 0.5 MeV. Therefore, the small Po-Be source spectra measurements made by Shook

(ref. 26) using the 1.2- by 1.3-centimeter cylindrical scintillator are believed to be one of the better resolved spectra for small (α, n) Be source reactions and serves as an estimate of the virgin source spectrum. This is discussed further in the following section, which describes the Am-Be source used in the present study.

Source

The present sphere transmission measurements were made with a large spherical Am-Be neutron source containing 54 Ci of ^{241}Am. The 16.7 grams of ^{241}Am was intimately mixed with 66.8 grams of Be powder, cold pressed, and contained in a net volume of 84.3 cubic centimeters. The compacts are doubly contained in two stainless steel shells, 0.140 and 0.152 centimeter thick, with an outer diameter of 6.10 centimeter and an inner diameter of 5.46 centimeter.

The source was calibrated by the manganese bath activation method in January 1967 and the emission rate was found to be $(1.30 \pm 0.08) \times 10^8$ neutrons per second. The calculations reported herein are based on the measured neutron emission rate so that the comparison of the calculated and the measured neutron leakage fluxes from the various spheres are on absolute comparative bases.

Because of the large physical size of the Am-Be source used, the directly measured spectra for the larger source cannot be used as input data for the sphere calculations. It was necessary to represent explicitly the uniform source region geometry and its stainless-steel containers in the transport calculations. The multigroup calculations are therefore for a fixed source and employ a virgin (α, n)Be spectrum that is uniformly distributed throughout the source region. The virgin source spectrum was obtained from the scintillator spectra measurements of a small standard Po-Be source that was approximately 1.2 centimeter long and 1.3 centimeters in diameter and contained approximately 2 grams of Be (see ref. 26). These spectra are shown in figure 4 in which measurements by the small scintillator using differentiation analysis are compared with the spectrum measured by the calibrated FERDOR method (ref. 25) for the 5- by 5-centimeter scintillator. Comparison of the spectra indicates good agreement with the integral flux above 0.5 MeV to within 4 percent. However, there are clear indications of the better resolution for the smaller detector as discussed earlier; the source components near 10, 8, 7, and 3 MeV are better resolved by the small detector.

In the region from 1 to 2 MeV, a valley is indicated that has consistently shown up in other measurements of the Po-Be source spectra (refs. 29 and 30). Recent measurements at Oak Ridge (ref. 31) using liquid scintillators, showed essentially identical results for neutron spectra from small Pu-Be, Po-Be, and Am-Be sources and also indicated a valley in the 1 to 2 MeV region. Since the poorer resolution of all measurements

in this energy region cannot adequately define the neutron yields, a virgin (α, n)Be spectrum has been selected and is shown as the histogram in figure 4. This virgin spectrum follows the small scintillator measurements except for the valley in the 1 to 2 MeV range. Here, quite clearly, the poor resolution conceals the true minima because of the higher surrounding yields. It was necessary to adjust yields with the 1- to 2-MeV region to conform with the known resolution functions in this energy range.

The precision of the virgin spectrum is indicated by the error bars in the figure. These error bars represent ±1 standard deviation and are estimated from the counting statistics, the energy calibration uncertainty, and the estimated uncertainty in the scintillator response functions for the case of unfolded spectra.

A check on the validity of the virgin spectrum shown in figure 4 lies in the agreement obtained between measurements of the leakage flux spectra from the large Am-Be (α, n) source and the transport calculations of this leakage flux spectra using the virgin (α, n) spectrum as uniformly distributed input. This comparison is presented later.

TRANSPORT CALCULATIONS

Fast neutron transport in the spherical shells of test materials containing the spherical Am-Be neutron source is described in terms of the space and energy angular neutron flux that satisfies the Boltzmann transport equation. In order to provide an accurate description of this neutron leakage flux spectra for the present experiments, the time independent multigroup form of the transport equation in spherical geometry is employed. This equation is given by

$$\frac{\mu}{r^2}\frac{\partial}{\partial r}\left[r^2\varphi_g(r,\mu)\right] + \frac{1}{r}\frac{\partial}{\partial r}\left[(1-\mu^2)\varphi_g(r,\mu)\right] + \sigma_g(r)\varphi_g(r,\mu) = S_g(r)$$

$$+ \sum_{l=0}^{\infty}(2l+1)P_l(\mu)\sum_{g'}\sigma_s^l(r, g' \to g)\varphi_{g'}^l(r) \qquad (1)$$

where

$$g = 1, 2, \ldots, G \quad \text{and} \quad -1 \le \mu \le 1$$

The notation used is conventional; in particular, σ_g is the macroscopic total cross section for group g and $S_g(r)$ is the isotropic fixed source term representing the neutrons originating from the Am-Be(α, n) reaction.

The quantity $\varphi_g(r, \mu)$ is the angular flux for group g at position r for neutrons moving in the cone of directions μ to $\mu + d\mu$ where μ is the cosine of the angle between the neutron direction of travel $\vec{\Omega}$ and the radius r of a sphere. The angular flux is expanded in a series of Legendre polynomials as

$$\varphi_g(r, \mu) = \sum_{l=0}^{\infty} (2l + 1)\varphi_g^l(r)P_l(\mu) \tag{2}$$

The coefficients $\varphi_g^l(r)$ in the expansion for the angular flux are given by

$$\varphi_g^l(r) = \frac{1}{2}\int_{-1}^{1} \varphi_g(r, \mu)P_l(\mu)\, d\mu \qquad l = 0, 1, 2, \ldots \tag{3}$$

where $P_l(\mu)$ is an lth order Legendre polynomial of argument μ.

The scalar flux $\Phi_g(r)$ is given by equation (3) for $l = 0$; that is,

$$\Phi_g(r) \equiv \varphi_g^0(r) = \frac{1}{2}\int_{-1}^{1} \varphi_g(r, \mu)\, d\mu \tag{4}$$

The net neutron current along a radius of a sphere $J_g(r)$ is given by equation (3) for $l = 1$; that is,

$$J_g(r) \equiv \varphi_g^1(r) = \frac{1}{2}\int_{-1}^{1} \varphi_g(r, \mu)\mu\, d\mu \tag{5}$$

The $\sigma_s^l(g' \to g)$ are coefficients in the expansion in a Legendre series of $\sigma_s(g' \to g, \mu_L)$, which is the probability per unit path length of a neutron scattering from group g' to group g through an angle μ_L where μ_L is the cosine of the angle between the initial and final directions of motion of a scattered neutron. This expansion for $\sigma_s(g' \to g, \mu_L)$ is given by

$$\sigma_s(g' \to g, \mu_L) = \sum_{l=0}^{\infty} \frac{2l + 1}{4\pi}\sigma_s^l(g' \to g)P_l(\mu_L) \tag{6}$$

The lth order group transfer coefficients includes elastic scattering and, if present,

inelastic scattering and the (n, 2n) reaction. The inelastic scattering and (n, 2n) reaction are usually included only for the $l = 0$ term.

Multigroup Solutions

Given the basic group cross sections for the materials involved in an experiment, the source spectrum, and the arrangement of the materials in spherical shells, a solution to equation (1) is obtained with the use of a computer. A solution to equation (1) consists of obtaining the discrete values of the angular flux $\varphi_g(r_i, \mu_m)$ for group g at position r_i and direction μ_m that approximate the angular flux $\varphi_g(r, \mu)$. This approximate solution to equation (1) is obtained by using a code based on the discrete ordinates S_n method that is a descendant of the DTF-IV code (ref. 32). Since the angular flux is expected to be anisotropic for this geometric arrangement of neutron source and spherical shells of test materials (i.e., the angular flux is expected to be forwardly directed), 16 directions μ_m were chosen to represent the angular flux. The 16 directions (comprising the S_{16} calculation) were obtained from the Gauss-Legendre quadrature set. The adequacy of this S_{16} quadrature set was tested by comparing the computed leakage spectra for the Ta sphere experiment with the results obtained for an S_{32} quadrature set; excellent agreement was obtained between the two calculations with the S_{16} calculation differing by less than 1 percent for all energy groups from the more accurate S_{32} calculation.

Microscopic cross section data for all of the test materials except W were obtained from the ENDF/B version III data files. These data were processed using a version of the SUPERTOG code (ref. 33) for the group split shown in table II excluding the thermal group (group 67). This 67 energy group split was chosen so that the energy width of the group was much less than the resolution of the liquid scintillator spectrometer and made the cross section averaging procedures insensitive to the assumed averaging spectra. Elastic scattering cross sections were included through the $l = 3$ term of the scattering source term on the right side of equation (1). Any inelastic scattering and (n, 2n) reaction cross sections were treated through the $l = 0$ term; that is, these two types of neutron scattering were assumed to be isotropic in the laboratory coordinate system.

For the W sphere the version of SUPERTOG that was available was not able to process all of the necessary data files. Therefore, the W data were obtained from the GAM-II code (ref. 34). The basis for the data in the GAM-II data files is reference 35. Fifty-one energy groups were used with the first 49 being the first 49 energy groups of the GAM-II code that covered the energy range from 14.9 to 0.11 MeV, with each group having a lethargy width of 0.1. The 50th and 51st groups of this energy group split were the same as the 66th and 67th of the 67 energy group split. This 51 energy group split

is unsatisfactory at the high energy end as the group width is of the order of the spectrometer resolution.

The thermal group for all of the materials used in this program were obtained from the GATHER-II code (ref. 36). Although the neutron groups below 0.1 MeV are not needed for comparison of the calculated neutron leakage spectra with the measurements obtained with the spectrometer, they are needed to complete the problem description. This permits an assessment of the neutron balance tables for any code malfunctions.

When performing calculations with the discrete ordinates S_n method, the highest order l used in the scattering source term of equation (1) defines a P_l calculation. The calculations made herein are thus P_3 calculations. A calculation for the Ta sphere experiment indicated that a lower order P_1 treatment of elastic scattering was adequate for computing the neutron leakage spectra. A comparison with the neutron leakage spectra computed for a P_3 treatment of elastic scattering indicated that the results for a P_1 calculation differed from those of a P_3 calculation by less than 2 percent for all groups. For all of the metallic test materials, similar results were obtained. The adequacy of the P_1 calculation is due to the dominance of the inelastic scattering and, in the case of Be, the (n, 2n) reaction rather than elastic scattering is responsible for the removal of neutrons from one energy to a lower energy region. On the other hand, a P_3 treatment of elastic scattering was necessary for the CH_2 sphere. Therefore, since the scattering order does not appreciably affect computer time, all calculations reported herein were performed with a P_3 treatment of elastic scattering to insure maximum accuracy.

Smoothed Leakage Spectra

For direct comparison of the multigroup calculations with the liquid scintillator spectrometer measurements of the neutron leakage spectra at 2 meters from the center of the test spheres, the multigroup results are smoothed using the known resolution function. The known Am-Be source strength of $1.30 \pm 0.08 \times 10^8$ neutrons per second is used for the calculations. The spectrometer measurements have been reduced by the FERDOR code (ref. 27), and the data are given as a differential flux in units of neutrons per square centimeter per second per MeV. Two methods of obtaining the calculated differential flux at the detector position are feasible. In the first method the flux is calculated directly by the S_n method from the source to the detector. This method results in a large number of spatial mesh points in the intervening region and a corresponding increase in the computing time. With this method the calculated differential flux is given as (method 1)

$$\Phi(r_d, E) = \sum_{g=1}^{G} \left[\Phi_g(r_d)/\Delta E_g\right] p(E_g \rightarrow E)\, \Delta E \tag{7}$$

where

$$p(E_g \rightarrow E)\, \Delta E = \frac{1}{\sqrt{\pi\sigma^2}} \exp\left[\frac{-(E_g - E)^2}{2\sigma^2}\right] \Delta E \tag{8}$$

In equation (7) $\Phi_g(r_d)$ is the scalar flux for group g at the detector position r_d, ΔE_g is the energy width of group g in MeV, $p(E_g \rightarrow E)\, \Delta E$ is the probability that an event at energy E_g will yield a response in ΔE about energy E, and σ is the energy resolution of the spectrometer in MeV corresponding to the full width at half-maximum of the Gaussian distribution. In equation (7) the summation extends over G groups where the 67 groups may be subdivided into a larger number of groups for this folding procedure.

In the second method the neutron differential flux at the detector position is calculated from the neutron leakage computed at the surface of the spherical assemblies assuming a $1/r^2$ spatial dependence; that is, $\Phi(r_d, E)$ is given by (method 2)

$$\Phi(r_d, E) = \sum_{g=1}^{G} \frac{\left[L_g(r_s)/\Delta E_g\right]}{4\pi r_d^2} p(E_g \rightarrow E)\, \Delta E \tag{9}$$

In equation (9) $L_g(r_s)$ is the number of neutrons in group g escaping from the surface of a spherical assembly that has an overall radius of r_s.

For the smaller spheres of the test materials, calculations indicate that the two methods for calculating the differential flux at the detector position give essentially the same results. For the two larger spheres (Pb and CH_2), the two methods differ by about 5 percent at energies greater than 5 MeV.

Sensitivity Calculations

An important factor in judging the utility of a comparison between the present sphere experiments and transport calculations is the sensitivity of the comparison to changes in cross sections of interest. For the high energy region considered here these are the total and nonelastic cross sections and the inelastic down scattering model. Several calcula-

tions have been made to estimate these sensitivities. Although they were made for specific spheres, the results are expected to correlate well with the thicknesses of spheres in mean free paths that are shown in table I.

For example, a calculation of the effect of increasing the total cross section for the Ta sphere by 10 percent resulted in only a 2- to 3-percent reduction in the leakage fluxes. On the other hand, a 10 percent increase in the nonelastic cross section while keeping the total cross section constant resulted in a 10- to 12-percent reduction in the leakage fluxes. Corresponding calculations made for the smaller Mo sphere indicated that these relative sensitivities were similar but were reduced approximately in proportion to the reduced sphere thickness in mean free paths.

The sensitivity of the comparison to the inelastic down scattering model is more difficult to estimate, but the sensitivity of calculated spectra to the evaporation model parameter used in the energy dependent temperature for continuum scattering was evaluated for one case. In the evaporation model the energy distribution of inelastically scattered neutrons is proportional to

$$N(E' \rightarrow E) \propto E\left[\exp\left(-\frac{E}{\theta}\right)\right]$$

where E' is the incident neutron energy and θ is the temperature of the residual nucleus approximated by the parameter $\sqrt{E'/a}$.

For the case of the Ta sphere, the parameter a was reduced by 50 percent, and the consequent increase in effective temperature resulted in a 35-percent increase in the leakage flux about the 2-MeV region. This result is illustrated later.

In summary, then, fixed source calculations were made in spherical geometry using 67 energy groups, an S_n quadrature order of 16 and a P_l elastic scattering order of 3. The calculations are on an absolute basis and are directly comparable with the measured differential energy flux at the detector position. The high order of the calculation assures that, within the uncertainties in the absolute source strength, the density of the various materials, and the dimension of the spherical shells, any differences between the calculated and measured spectra can be attributed to inadequacies in high energy neutron cross sections.

DISCUSSION OF RESULTS

The measured neutron leakage flux spectra at 2 meters from the bare Am-Be source and for this source at the center of various spheres of test materials are presented. The absolute measurements are compared with the absolute transport calculation of the same quantity employing the known source strength and the virgin Be(α,n) source spectrum

uniformly distributed within the large Am-Be source. For the convience of others who may wish to compare their calculations with the present sphere measurements, the measured results are listed on table III.

Bare Americium-Beryllium Source

The comparison of measured and calculated leakage flux spectra for the bare Am-Be source in air is presented in figure 5. The measured results are shown by the vertical bars that represent ±1 standard deviation that is estimated from the counting statistics, the energy calibration uncertainty, and the uncertainty of the FERDOR response functions.

In order to facilitate direct comparison of the calculations with the measured neutron flux per MeV at 2 meters, the calculated multigroup flux per MeV at 2 meters has been smeared by the known resolution function of the NE213 liquid scintillator and the results appear as the solid line.

The large source used has sufficient Be and Fe to modify the virgin (α, n) spectrum; ENDF/B cross sections have been used for these elements. The effects of Fe are small but the contributions of (n, 2n) reactions with Be are calculated to result in a net enhancement of source strength by 4.2 percent in excess of the distributed virgin source input. To satisfy conservation, calculations were therefore based on a distributed virgin source strength 4.2 percent less than the measured strength of the Am-Be source. The comparison of leakage spectra for the bare Am-Be source is shown in figure 5 and indicates excellent absolute agreement with calculations over the entire measured range. Quite clearly the resolution function of the scintillator spectrometer has smoothed out the prominences of the input spectra but the shapes and magnitudes agree.

Beryllium

The most important high-energy reaction in Be that affects downscattering is the (n, 2n) reaction. It is the comprehensive work by Perkins (refs. 37 and 38) that presents a detailed model for this reaction and provides data for the angular and energy distributions for neutrons from the various decay modes of the process. An early integral test of these cross sections was presented by Alexander, Fieno, and Ford (ref. 39), where the slowing down flux was measured in a water medium that contained an Am-Be source enclosed in Be spheres. The superiority of the Perkins data over other sets was demonstrated.

The Perkins models are incorporated in the ENDF/B evaluation for Be (MAT 1154), and this has been used in the present calculations. However, in the multigroup cross

section preparation by SUPERTOG, the energy-angle correlations available in the evaluated data for the (n, 2n) reaction are neglected. In the present calculations, the effects of ignoring and preserving this angular correlation were studied by (1) using ENDF/B cross sections as processed by SUPERTOG and (2) calculating and using group cross sections and transfer matrices by the AGN-SIGMA code (ref. 40). In the second calculation, the energy-angle correlation for the two branches of the Be(n, 2n) reaction via the 2.43-MeV level were represented to P_1 order rather than P_0 order.

The partial cross sections due to the 2.43-MeV level dominate the (n, 2n) reaction above 4 MeV in the Perkins model as shown in figure 6. The majority (91.7 percent) of these reactions are assigned as leaving ^{8*}Be in a broad 2.90-MeV excited state with an effective excitation energy in ^{8}Be of 0.6 MeV. The smaller fraction (8.3 percent) goes to the ground state of ^{8}Be. Partial cross sections for the excitation of levels in ^{9*}Be at 6.76 and 9.1 MeV are also assigned by Perkins. The remaining cross section, which is a large fraction of the (n, 2n) cross section at lower energies, proceeds by multibody breakup.

The experimental leakage flux spectrum for the Am-Be source enclosed in the 20-centimeter-diameter Be sphere is shown in figure 7 and compared with the two calculated spectra. The solid curve is based on the data of ENDF/B (MAT 1154). The data agree well above 4 MeV but a persistent underprediction below this energy is noted. However, inclusion of the P_1 component in the (n, 2n) scattering matrix results in a definite improvement between calculation and experiment in this region, and is therefore important for fast spectra studies in Be. For this source-sphere configuration, (n, 2n) reactions in the beryllium sphere result in an additional calculated net source enhancement of 26.6 percent.

Polyethylene

The results for the polyethylene sphere serve as a partial check of the absolute precision of the present experimental technique. The leakage flux spectra at 2 meters are shown in figure 8, where measurements are compared with the transport calculations using ENDF/B data for H (MAT 1148) and C (MAT 1165). Although the hydrogen cross sections serve as a standard and the total cross sections for carbon qualify as standards, the nonelastic cross sections for carbon are not as well known.

The transport calculations for the leakage flux spectra from the surface of this sphere to the detector point at 2 meters have been made by the two methods discussed earlier. These results are shown in figure 8. Here, the dashed line represents the flux directly calculated by the P_3S_{16} discrete ordinate approximation from the sphere through the intervening void to the detector position at 2 meters. The solid line repre-

sents the leakage flux at the detector position computed from the discrete ordinate fluxes at the surface of the sphere by summing over the surface of the sphere and using a $1/r^2$ variation from the local surface to the detector. It is this method that has been used for the smaller spheres measured.

The two methods of calculation to the detector agree within a few percent over the entire range of energy as they may be expected to since the detector point is of the order of 10 radii from the surface of the sphere.

The agreement of measured and calculated absolute flux spectra above 2 MeV is excellent. The oscillations in the measured spectra below 4 MeV are not as well followed but are averaged quite well by the calculations. The discrepancy that appears below 1 MeV is significant and may be due to inadequate downscattering matrices for the inelastic partial cross sections of carbon.

Lead

The case of the natural Pb sphere serves as a graphic example of the improvement in high-energy inelastic cross sections brought about by comprehensive evaluation techniques. Until the recent evaluation of natural Pb by Fu and Perey (ref. 41) to provide ENDF/B data for MAT 1136, the earlier ENDF compilation for Pb designated MAT 43 represented the only available data to shield calculators and others. The new evaluation has separated the reasonably well measured total nonelastic cross section into analytical partial cross sections. (See figure 9, which is reproduced from ref. 41.) The calculated components and the measured total nonelastic cross section agreed so well that the calculated results were adapted by the evaluators.

The measured and calculated sphere leakage flux spectra at 2 meters from the natural Pb sphere is shown in figure 10. A preliminary analysis of these data was presented in reference 24. The calculations using MAT 43 are significantly lower than the measurements below 7 MeV and rise above the data below 0.7 MeV. The comparison is particularly poor at 2 MeV where the calculated flux using MAT 43 is half of the measured flux. On the other hand the calculations using the later evaluation of MAT 1136 shows considerable improvement below 3 MeV. However, the calculations using MAT 1136 result in about a 20-percent underprediction in the energy range from 3 to 6 MeV, which suggests that further improvement in the recent evaluation for Pb is required.

Niobium

Nb represents a material of great interest to reactors and for which the cross sec-

tions have undergone several revisions since the initial evaluation by Allen and Drake (ref. 42). In late 1971 new data suggested the reduction of the inelastic cross sections below 1.5 MeV and above the (n, 2n) threshold and corresponding increase in the (n, 2n) cross section. Individual inelastic levels are delineated up to 1.4 MeV with a continuum assigned above 1.4 MeV based on an assigned nuclear temperature. The ENDF/B evaluated cross section set used is updated MAT 1164.

The measured and calculated leakage flux spectra at 2 meters from the 25-centimeter-diameter Nb sphere are shown in figure 11. The calculations using MAT 1164 data are in reasonably good agreement with the measurements at the higher and lower energies but underestimate the measured fluxes from 3 to 6 MeV and fail to represent the apparent structure in the measured spectra around 2 to 3 MeV.

Molybdenum

The myriad of isotopes of Mo make evaluation of the average elemental cross sections a difficult task. The basis for ENDF/B cross sections for natural Mo is the evaluation of Pennington and Gajniak (ref. 43) designated as MAT 1111. The high-energy cross sections of interest here are based on a combination of measurements and optical model calculations for elastic scattering angular distributions and on measurements of four resolved inelastic levels below 1.5 MeV and assigned nuclear temperatures for the (n, n'), (n, 2n), and (n, 3n) reactions. The evaluation was revised by Pennington in January 1972.

The measured and calculated leakage flux spectra at 2 meters from the Mo sphere are shown in figure 12. The agreement between experiment and calculations is generally satisfactory and similar in quality to that observed for the bare source. The Mo sphere leakage spectra is considerably softer than that of the bare source of course. As noted in table I, the Mo sphere is the smallest sphere measured, and the shell thickness corresponds to but 0.8 total mean free path at 4 MeV.

Sensitivity calculations for this shell thickness indicate that a 10-percent change in the total inelastic cross section will change the flux 5 percent, which is slightly smaller than the experimental error of ±7 percent. On the basis of these present data, we conclude that the ENDF/B data for high-energy cross sections of Mo represents this element very well.

Tantalum

Tantalum represents a case for which a new ENDF/B evaluation has become avail-

able and for which the present sphere measurements represent an opportunity to compare two successive ENDF/B sets of cross sections. The present Ta sphere measurements were first presented in reference 23 and compared with the earlier ENDF/B data compiled as MAT 1035 evaluated by Prince (ref. 44) and by Henderson, DeCorrevant, and Zwick (ref. 45).

A comparison of measured and calculated leakage flux spectra at 2 meters for the Ta sphere is shown in figure 13. The calculations using the data compilation MAT 1035 significantly underestimates the measured fluxes for energies less than 4 MeV. Since the parameter a used in the evaporation model of the inelastic continuum has a strong effect on the spectra, the value was changed from that used in MAT 1035. The modification consisted of changing the parameter a in the evaporation model from 25 MeV^{-1} to 12 MeV^{-1}, which resulted in effectively higher temperatures. A significant improvement is achieved with considerably better agreement below 6 MeV. However, there is no assurance that the calculated spectra are improved below 0.5 MeV, the limit of the present measurements. Above 6 MeV the calculations with MAT 1035 data are consistently higher than the measurements. This is attributed to smoothed inelastic cross sections that are lower than the measured isolated inelastic cross sections.

A recent reevaluation of Ta data (ref. 46), which has been adopted by ENDF/B as MAT 1126, has considered the inelastic cross sections in detail. The total nonelastic cross sections and the smoothed curves used in the two evaluations are shown in figure 14. With the exception of an isolated data point by Owens, all inelastic data points lie between the curves. Although MAT 1035 underestimates the data, MAT 1126 appears to overestimate it and results in about a 25-percent difference between the two curves over most of the high-energy region.

The third calculated curve in figure 13 was generated using the more recent ENDF/B data of MAT 1126. This calculated curve is significantly below the sphere spectra measurements at all energies. There are two possible reasons for these discrepancies. The first is due to the comparison in figure 14 where it is shown that the total nonelastic cross sections for the evaluation of MAT 1126 is significantly higher than the data. This appears to be the more likely reason for the lower flux spectra above 6 MeV calculated for the Ta sphere using MAT 1126. Therefore a smoothed curve of the nonelastic data intermediate between the evaluations of MAT 1035 and MAT 1126 would satisfy the present sphere spectra measurements. The second reason appears to be the poorly chosen value of the evaporation model parameter a.

These results were communicated to the evaluators of MAT 1126 and a reply by Ottewitte (unpublished document entitled "Angular Distribution of Neutrons Inelastically Scattered from ^{181}Ta") suggested that a possible cause of the low sphere leakage flux spectra that was calculated may have been due to the neglect of anisotropy in inelastic scattering. The data of both MAT 1035 and MAT 1126 specify isotropy for inelastic

scattering processes. In order to estimate the effect of anisotropy, Ottewitte made calculations for the 136-keV inelastic level of ^{181}Ta, which indicated significantly increasing anisotropy above ~6 MeV. Unfortunately, these data could not be included in the present transport calculations for the sphere. However, calculations for comparable effects of anisotropy have been made for the case of Be as previously discussed. In that case it was shown that consideration of anisotropy for partial (n, 2n) cross sections did raise the calculated flux spectra but the effects were limited to energies less than 3 MeV as shown in figure 7. For the case of Ta this finding would also be true since the inelastic reactions in the continuum region result, in general, in large energy losses that effectively remove neutrons from the region above ~3 MeV. Therefore, consideration of anisotropy for Ta would be expected to result only in an increase in calculated fluxes below ~3 MeV and would not greatly affect calculated fluxes above this energy.

It is concluded that, although the newer evaluations (ref. 46) are based on more complete and more accurate data than were available for the previous evaluation (refs. 44 and 45) and more sophisticated optical model calculations were performed, there is still room for improvement. A process of iteration to include the results of integral experiments such as those reported herein can lead to more accurate high-energy cross sections.

Tungsten

Available compilations of cross sections for W and its isotopes are relatively old and are in process of reevaluation by members of the Cross Section Evaluation Working Group of Sigma Center at the Brookhaven National Laboratory. The evaluation by Joanou and Stevens (ref. 35) has been used to interpret the present sphere measurements. In figure 15 the high-energy data from this evaluation are compared with the data evaluated by Prince (ref. 44) and by Henderson, DeCorrevant, and Zwick (ref. 45) that presently comprise the ENDF/B files as MAT 1060 (W-182), MAT 1061 (W-183), MAT 1062 (W-184), and MAT 1063 (W-186). These isotopic data were updated in 1970 by Prince.

Both sets of calculated data employed the individual partial inelastic cross sections for the same identified isotopic levels below 1.5 MeV. Both employed the measured elemental total and elastic cross sections for the individual isotopes. Both employed optical model calculations at higher energies and an assigned value of the parameter a to define neutron emission spectra for the continuum and identical values of a were used for all isotopes. Cross sections for (n, 2n) processes were analytically derived above the 8-MeV threshold in both cases. The two sets of cross sections for total, elastic, inelastic, and (n, 2n) cross sections that are compared in figure 15 indicate significant differences in all cross sections. As mentioned before, the verson of

SUPERTOG (ref. 33) that was available was unable to process the necessary ENDF/B data listings for tungsten. Therefore, the data used were obtained from the GAM II set (ref. 34). It is unfortunate that a comparison with the Prince and Henderson evaluation was not possible.

The measured and calculated leakage flux spectra at 2 meters from the two W spheres are shown in figures 16 and 17. In both cases a significant and consistent underestimate of the measured spectra is calculated below 6 MeV; above this energy the data are in better agreement. Although the fewer group calculations do not represent adequately the source shape at 8 and 10 MeV, this does not affect the spectra at lower energies very much. It is suggested that new evaluations of W be compared with the present experimental data, tabulations of which are listed in table III.

SUMMARY OF RESULTS

A summary and comments on comparison of the measured and calculated sphere leakage spectra are presented in the following table:

Material	Figure	ENDF/B MAT	Comments
Beryllium	7	1154	Data agree well above 4 MeV. Consideration of anisotropy in (n, 2n) reaction component improves results below 4 MeV.
Polyethylene	8	1148(H) 1165(C)	Excellent agreement above 2 MeV. Discrepancy below 1 MeV attributed to carbon down scattering model.
Lead	10	1136	Generally good agreement but some underprediction from 3 to 6 MeV suggests further improvement in down-scattering model required.
Niobium	11	1164	Good agreement above 7 MeV and below 2 MeV. Calculations underestimate data at intermediate energies significantly.
Molybdenum	12	1111	Good agreement over entire range of energy.
Tantalum	13	1126	Poor agreement over entire range of energy. Discrepancy above 5 MeV attributed to incorrect inelastic cross section magnitude; below 5 MeV to inadequate treatment of continuum and neglect of anisotropy of inelastic scattering.
Tungsten-182	16 and 17	1060	Early evaluations have not incorporated more recent data and are in process of reevaluation. GAM II data inadequate below 6 MeV. (ENDF/B data not explicitly used.)
Tungsten-183	↓	1061	
Tungsten-184	↓	1062	
Tungsten-186	↓	1063	

Lewis Research Center,
National Aeronautics and Space Administration,
Cleveland, Ohio, August 8, 1973,
503-10.

REFERENCES

1. Hemmig, P. B.: Development of the ENDF/B System. Third Conference on Neutron Cross Sections and Technology. AEC Rep. CONF-710301, Vol. 1, 1971, p. 348.

2. Hummel, H. H.: Sensitivity Studies of the Effect of Uncertainty in the $^{238}U(n,\gamma)$ and in the $^{239}Pu(n,f)$ and (n,γ) Cross Sections. Third Conference on Neutron Cross Sections and Technology. AEC Rep. CONF-710301, Vol. 1, 1971, p. 65.

3. Drake, M. K., ed.: ENDF/B-III Cross Section Measurement Standards. Rep. BNL 17188 (ENDF-179), Brookhaven National Lab., 1972.

4. Carlson, A. D.: Neutron Capture Cross Section Standards. Symposium on Neutron Standards and Flux Normalization. AEC Rep. CONF-701002, 1970, p. 285.

5. Poenitz, W. P.: Absolute Cross Sections of ^{197}Au and ^{238}U. Symposium on Neutron Standards and Flux Normalization. AEC Rep. CONF-701002, 1970, p. 320.

6. Landon, H. H.: Present Status of Standards. Third Conference on Neutron Cross Sections and Technology. AEC Rep. CONF-710301, Vol. 2, 1971, p. 528.

7. Davey, W. G.: An Analysis of the Neutron Capture Cross Section of ^{238}U Between 1 keV and 15 MeV. Nucl. Sci. Eng., vol. 39, no. 3, Mar. 1970, pp. 337-360.

8. Orphan, V. J.: Measurement and Evaluation of Cross Sections. Topical Meeting on New Developments in Reactor Physics and Shielding. AEC Rep. CONF-720901, Book 1, 1972.

9. Perey, F. G.; Kinney, W. E.; and Macklin, R. L.: High Resolution Inelastic Cross Section Measurements for Na, Si, and Fe. Third Conference on Neutron Cross Sections and Technology. AEC Rep. CONF-710301, Vol. 1, 1971, p. 191.

10. Schmitt, H. W.; and Cook, C. W.: Absolute Neutron Absorption Cross Sections for Sb-Be Photoneutrons. Nucl. Phys., vol. 20, 1960, pp. 202-219.

11. Bogart, D.; and Semler, T. T.: Monte Carlo Interpretation of Sphere Transmission Experiments for Average Capture Cross Sections at 24 keV. Conference on Neutron Cross Section Technology. AEC Rep. CONF-660303, Book 1, 1966, p. 502.

12. Miller, L. B.; and Poenitz, W. P.: Monte Carlo Interpretation of a ^{238}U Spherical Shell Transmission Experiment at 23 keV. Nucl. Sci. Eng., vol. 35, no. 2, Feb. 1969, pp. 295-297.

13. Semler, Thor T.: Effect of Multiple Spin Species on Spherical Shell Neutron Transmission Analysis. J. Nucl. Energy, vol. 27, no. 3, Mar. 1973, pp. 185-191.

14. Maienschein, F. C.; Clifford, C. E.; Mynatt, F. R.; and Abbott, L. S.: Shielding for Advanced Reactors in the United States. Nucl. Eng. Design, vol. 15, 1971, pp. 241-264.

15. Alter, Harry: ENDF/B-2: Is It Adequate for the Design and Evaluation Needs of the LMFBR Program? Reactor Tech., vol. 15, no. 1, Spring 1972, pp. 59-75.

16. Profio, A. E., ed.: Shielding Benchmark Problems. Rep. ORNL-RSIC-25, ANS-SD-9, Oak Ridge National Lab., June 1969.

17. Straker, E. A.: Integral Experiments and Philosophy of Benchmark Calculations. Topical Meeting on New Developments in Reactor Physics and Shielding. AEC Rep. CONF-720901, Book 1, 1972, p. 350.

18. Davey, William G.; and Amundson, Paul I.: Inelastic Scattering Measurements in a Fast Reactor by the Spherical Shell Method. Nucl. Sci. Eng., vol. 28, no. 1, Apr. 1967, pp. 111-123.

19. Clifford, C. E.; Straker, E. A.; Muckenthaler, F. J.; Verbinski, V. V.; Freestone, R. M., Jr.; Henry, K. M.; and Burrus, W. R.: Measurements of the Spectra of Uncollided Fission Neutrons Transmitted Through Thick Samples of Nitrogen, Oxygen, Carbon, and Lead: Investigation of the Minima in Total Cross Sections. Nucl. Sci. Eng., vol. 27, no. 2, Feb. 1967, pp. 299-307.

20. Straker, E. A.: Experimental Evaluation of Minima in the Total Neutron Cross Sections of Several Shielding Materials. Nucl. Sci. Eng., vol. 34, no. 2, Nov. 1968, pp. 114-121.

21. Profio, A. E.; Cerbone, R. J.; and Huffman, D. L.: Fast Neutron Penetration in Paraffin and Lithium Hydride. Nucl. Sci. Eng., vol. 44, no. 3, June 1971, pp. 376-387.

22. Cerbone, R. J.; Lathrop, K. D.: S_n Calculation of Highly Forward Peaked Neutron Angular Fluxes Using Asymmetrical Quadrature Sets. Nucl. Sci. Eng., vol. 35, no. 1, Jan. 1969, pp. 139-141.

23. Shook, D. F.; Fieno, D.; Ford, C. H.; and Alexander, R. L.: An Integral Test of Inelastic Scattering Cross Sections Using Measured Neutron Spectra from Thick Shells of Ta, W, Mo, and Be. Third Conference on Neutron Cross Sections and Technology. AEC Rep. CONF-710301, Vol. 1, 1971, p. 98.

24. Shook, D. F.; Fieno, D.; and Ford, C. H.: An Integral Test of the Inelastic Scattering Cross Sections of Pb and Mo Using Measured Spectra. Trans. ANS, vol. 15, no. 1, June 1972, p. 527.

25. Verbinski, V. V.; Burrus, W. R.; Love, T. A.; Zobel, W.; Hill, N. W.; and Textor, R.: Calibration of an Organic Scintillator for Neutron Spectrometry. Nucl. Instr. Methods, vol. 65, 1968, pp. 8-25.

26. Shook, Donald F.; and Pierce, Clarence R.: Comparison of Neutron Spectra Measured with Three Sizes of Organic Liquid Scintillators Using Differentiation Analysis. NASA TM X-2646, 1972.

27. Burrus, W. R.: Utilization of a Priori Information by Means of Mathematical Programming in the Statistical Interpretation of Measured Distributions. Rep. ORNL-3743, Oak Ridge National Lab. (NASA CR-63442), June 1965.

28. Shook, Donald F.; and Blue, James W.: Circuit Modification Aids in Atomic Particle Discrimination. NASA Tech Brief 70-10689, 1970.

29. Whitmore, B. G.; and Baker, W. B.: The Energy Spectrum of Neutrons from a Po-Be Source. Phys. Rev., vol. 78, no. 6, June 15, 1950, pp. 799-801.

30. Haag, D.; and Fuchs, H.: Die Energieverteilung der Neutronen aus einer Po-α-Be-Quelle. Zeit. f. Physik, vol. 174, 1963, pp. 227-230.

31. Freestone, R. M., Jr.; Muckenthaler, F. J.; Straker, E. A.; and Henry, K. M.: Measurements of the Neutron Spectra of Po-Be, Pu-Be, and Am-Be Neutron Sources with an NE213 Scintillator. Neutron Physics Division Annual Progress Report for Period Ending May 31, 1967. Rep. ORNL-4134, Oak Ridge National Lab., Aug. 1967, p. 25.

32. Lathrop, K. D.: DTF-IV, A FORTRAN-IV Program for Solving the Multigroup Transport Equation with Anistropic Scattering. Rep. LA-3373, Los Alamos Scientific Lab., Nov. 12, 1965.

33. Wright, R. Q.; Greene, N. M.; Lucius, J. L.; and Craven, W. W., Jr.: SUPERTOG: A Program to Generate Fine Group Constants and P_n Scattering Matrices from ENDF/B. Rep. ORNL-TM-2679, Oak Ridge National Lab. (AD-693232), Sept. 1969.

34. Joanou, G. D.; and Dudek, J. S.: GAM-II. A B_3 Code for the Calculation of Fast-Neutron Spectra and Associated Multigroup Constants. Rep. GA-4265, General Dynamics Corp., Sept. 16, 1963.

35. Joanou, G. D.; and Stevens, C. A.: Neutron Cross Sections for Tungsten Isotopes. Rep. GA-5885, General Dynamics Corp. (NASA CR-54261), Nov. 13, 1964.

36. Joanou, G. D.; Smith, C. V.; and Vieweg, H. A.: GATHER-II. An IBM-7090 FORTRAN-II Program for the Computation of Thermal-Neutron Spectra and Associated Multigroup Cross Sections. Rep. GA-4132, General Dynamics Corp., July 8, 1963.

37. Perkins, Sterrett T.: The $^{9}Be(n, 2n)$ Reaction and Its Influence on the Age and Fast Effect in Beryllium and Beryllium Oxide. Rep. AN-1443, Aerojet-General Nucleonics (AEC Rep. TID-22446), Oct. 1965.

38. Perkins, S. T.: A Calculation of the Angular and Energy Distributions for Neutrons from the $^{9}Be(n, 2n)$ Reaction. Rep. UCRL-50520, Lawrence Radiation Lab., Oct. 4, 1968.

39. Alexander, Roger L.; Fieno, Daniel; and Ford, C. Hubbard: Tests of Evaluated Beryllium (n, 2n) Cross Sections by Analysis of 1.4-eV Flux in Water for an Americium-Beryllium Source Enclosed in Beryllium Spheres. Nucl. Sci. Eng., vol. 44, no. 1, Apr. 1971, pp. 95-102.

40. Perkins, S. T.; Thompson, D. W.; and DuBois, P. J.: Users Manual for AGN-SIGMA: A Code to Calculate the Legendre Components of the Multigroup Transfer Matrices and the Group Cross Sections. Rep. AN-1447, Aerojet-General Nucleonics (AEC Rep. TID-22447), Oct. 1965.

41. Fu, C. Y.; and Perey, F. G.: An Evaluation of Neutron and Gamma-Ray-Production Cross Sections for Lead. Rep. ORNL-4765, Oak Ridge National Lab., Mar. 17, 1972.

42. Allen, M. S.; and Drake, M. K.: Neutron Cross Sections for Niobium. Rep. GA-8133, Add., Gulf General Atomic, Mar. 28, 1969.

43. Pennington, E. M.; and Gajniak, J. C.: Compilation of ENDF/B Data for Magnesium, Titanium, Vanadium, Molybdenum, and Gadolinium. Rep. ANL-7387, Argonne National Lab., Mar. 1968.

44. Prince, A.: Neutron Cross Sections for Tantalum and Tungsten. Rep. GEMP-388, General Electric Co., Nov. 10, 1965.

45. Henderson, W. B.; DeCorrevant, P. A.; and Zwich, J. W.: Evaluation and Compilation of Ta-181, W-182, W-183, W-184, and W-186 Cross Section Data for the ENDF/B File. Rep. GEMP-488, General Electric Co., 1966.

46. Ottewitte, E. H.; Otter, J. M.; Rose, P. F.; and Dunford, C. L.: An Evaluation of ^{181}Ta and ^{182}Ta for the ENDF/B Data File. Rep. AI-AEC-12990, Atomics International, Sept. 30, 1971.

47. Beyster, J. R.; Walt, M.; and Salmi, E. W.: Interaction of 1.0-, 1.77-, 2.5-, 3.25-, and 7.0-MeV Neutrons with Nuclei. Phys. Rev., vol. 104, no. 5, Dec. 1, 1956, pp. 1319-1331.

48. Walt, M.; and Beyster, J. R.: Interaction of 4.1-MeV Neutrons with Nuclei. Phys. Rev., vol. 98, no. 3, May 1, 1955, pp. 677-684.

49. Thomson, David B.: Nuclear Level Densities and Reaction Mechanisms from Inelastic Scattering. Phys. Rev., vol. 129, no. 4, Feb. 15, 1963, pp. 1649-1667.

50. Owens, R. O.; and Towle, J. H.: The Level Density of the Deformed Rare-Earth Nuclei. Nucl. Phys., vol. A112, 1968, pp. 337-359.

TABLE I. - COMPOSITION AND SIZE OF TEST SPHERES[a]

Material	Form	Density, g/cm^3	Outside diameter, cm	Container[b], cm	Shell thickness, cm	Shell thickness, total mean free paths at 4 MeV
CH_2	Polyethylene	0.957	45.72	-----	19.81	4.5
Be	Solid metal	1.84	20.32	-----	7.00	1.7
Nb	Solid metal	8.4	25.4	-----	9.61	2.0
Mo	Powder	3.73	22.96	(0.05)	8.38	.8
Ta	Solid metal	16.60	24.13	-----	9.02	3.4
W	Fine balls	11.87	22.96	(0.05)	8.38	2.0
W	Fine balls	12.26	44.24	(0.48)	18.29	4.5
Pb	Solid metal	11.35	38.0	-----	15.9	4.0

[a]All materials are chemically pure with impurities in the ppm range. Only the Nb sphere has a significant component of 0.95 percent by weight of Zr.

[b]Container material, stainless steel.

TABLE II. - ENERGY BOUNDARIES OF 67 GROUP SPLIT

Group	High-energy boundary of group, MeV	Energy width of group, MeV	Virgin source fraction	Group	High energy boundary of group, MeV	Energy width of group, MeV	Virgin source fraction
1	11.331	0.279	0.000330	37	3.867	0.188	0.029836
2	11.052	.273	.001699	38	3.679	.180	.033700
3	10.779	.266	.004010	39	3.499	.170	.032400
4	10.513	.260	.006221	40	3.329	.163	.026700
5	10.253	.253	.007526	41	3.166	.154	.023188
6	10.000	.247	.008642	42	3.012	.147	.021269
7	9.753	.241	.007721	43	2.865	.140	.018104
8	9.512	.235	.005624	44	2.725	.133	.015515
9	9.277	.229	.004591	45	2.592	.126	.013445
10	9.048	.223	.006684	46	2.466	.120	.012154
11	8.825	.218	.010140	47	2.346	.115	.009900
12	8.607	.212	.012271	48	2.231	.108	.008040
13	8.395	.208	.013867	49	2.123	.104	.007020
14	8.187	.202	.014402	50	2.019	.192	.011401
15	7.985	.197	.016120	51	1.827	.174	.006968
16	7.788	.192	.016170	52	1.653	.157	.006287
17	7.596	.188	.014484	53	1.496	.143	.006321
18	7.408	.183	.012698	54	1.353	.128	.006091
19	7.225	.178	.011839	55	1.225	.117	.007730
20	7.047	.174	.014082	56	1.108	.105	.008440
21	6.873	.170	.014806	57	1.003	.182	.017775
22	6.703	.165	.014282	58	.821	.149	.016573
23	6.538	.162	.013805	59	.672	.122	.015032
24	6.376	.157	.013378	60	.550	.100	.012457
25	6.219	.154	.013948	61	.450	.081	.010163
26	6.065	.149	.013832	62	.369	.067	.008391
27	5.916	.146	.015370	63	.302	.078	.009769
28	5.770	.143	.017200	64	.224	.058	.007264
29	5.627	.139	.017426	65	.166	.055	.006889
30	5.488	.267	.037562	66	.111	.111	.014036
31	5.221	.255	.038803	67	[a] $.414\times10^{-6}$	$.414\times10^{-6}$	0
32	4.966	.242	.037056				$\Sigma = 1.000000$
33	4.724	.231	.038848				
34	4.493	.219	.036369				
35	4.274	.208	.034159				
36	4.066	.199	.031177				

[a]Lower energy limit is 0.0001 eV.

TABLE III. - MEASURED ABSOLUTE NEUTRON LEAKAGE SPECTRA AT 2 METERS

FROM SPHERES CONTAINING Am-Be SOURCE

Energy, MeV	Bare source	Beryllium	Polyethylene (CH_2)	Lead	Niobium	Molybdenum	Tantalum	Tungsten	
								Small	Large
	Absolute neutron leakage spectra, neutrons/cm^2-sec-MeV								
0.4	--------	--------	14.5±5.5	---------	---------	--------	--------	--------	280±40
.5	44±4	71±6	10.0±4	160±10	190±20	93±8	--------	--------	165±30
.6	40±3	65±6	9.5±2.5	150±10	165±20	84±6	--------	--------	140±20
.7	39±3	54±5	7.5±2.7	135±7	147±15	75±6	--------	--------	105±15
.8	36±3	48±4	5.5±0.7	120±7	110±10	65±5	86±9	92±8	74±11
.9	35±3	48±4	3.9±0.7	115±7	91±9	61±5	70±8	85±8	70±8
1.0	33±3	48±4	3.9±0.7	100±6	72±8	56±5	60±7	75±7	57±8
1.1	28±2	47±4	4.2±0.7	95±5	56±5	52±5	52±6	66±7	46±8
1.2	24±2	49±4	4.0±0.6	85±5	48±5	50±4	43±3	58±6	34±7
1.3	24.5±2	51±3	3.9±0.6	78±5	39±4	47±4	37±3	49±6	29±5
1.4	25±2	52±3	3.85±0.5	73±5	29±3	43±4	31±2.5	41±5	23.5±4
1.5	23±2	52±3	3.6±0.5	65±4	24±3	39±4	24.5±2.5	35±4	18.5±4
1.6	21.5±2	51±3	3.3±0.4	58±3	24.5±3	36.5±3	21.5±2	29±3	15.5±3
1.7	21.5±2	48±3	3.25±0.4	55±3	26.5±2	35±3	19±2	26±2	12.5±2
1.8	23±2	46±3	3.55±0.4	52±3	26.5±2	34±3	17±2	24.5±2	10.0±1.5
1.9	25±2	44±3	3.8±0.4	50±3	24.5±2	33±3	15.5±1.5	24.5±2	9.0±0.9
2.0	28±2	42.5±2.5	4.0±0.4	49±3	23±2	32±2.5	14±1.5	23.5±2	8.3±0.9
2.1	30±2.5	41±2.5	3.8±0.4	46±3	21±2	32±2.5	12.5±1	22.0±1	7.4±0.8
2.2	32±3	39±2.5	3.5±0.4	42±2	20±1.5	31.5±2.5	12.2±1	19.5±1	6.1±0.7
2.3	32.5±3	37±2.5	3.3±0.4	36.5±2	17.7±1.5	30.5±2.5	11.2±0.8	17.5±1	5.5±0.7
2.4	33±3	35±2	3.3±0.4	33.0±1.5	16.5±1.5	29.5±2.5	10.5±0.8	16.0±1	5.3±0.7
2.5	34±2.5	31±2	3.5±0.4	28.5±1.5	15.3±1.5	29.0±2	9.5±0.6	15.7±0.8	5.4±0.6
2.6	35±2.5	27.5±1.5	3.7±0.4	25.5±1.5	14.0±1.5	29.5±2	9.5±0.6	15.2±0.8	5.4±0.6
2.7	35±2.5	23±2	3.8±0.4	24.0±1.5	15.0±1.5	29.0±2	9.5±0.6	16.0±0.8	5.1±0.5
2.8	36±2	21.5±1.5	3.8±0.4	22.0±1.5	15.2±1.5	28.0±2	9.5±0.6	16.2±0.8	4.9±0.5
2.9	36±2	20±2	3.65±0.4	21.5±1.5	16.5±1.5	28.0±2	9.5±0.6	16.4±0.8	4.9±0.5
3.0	36.5±2	18.5±1.5	3.45±0.35	20.5±1.5	17.0±1.5	27.5±2	9.5±0.6	16.4±0.8	4.8±0.5
3.2	37±2	18.5±1.5	3.3±0.35	18.5±1.5	17.0±1.5	26.5±2	9.4±0.5	16.5±0.7	4.5±0.5
3.4	35±2	18.5±1.5	2.9±0.30	16.5±1.5	15.2±1.5	26.5±2	9.0±0.5	16.5±0.7	4.3±0.4
3.6	35±2	18.5±1.5	2.45±0.25	14.5±1	13.5±1.0	26.5±2	8.9±0.4	16.4±0.7	4.3±0.4
3.8	37±2	19±1	2.65±0.25	13.2±1	12.7±1.0	26.0±2	8.9±0.4	16.3±0.7	4.2±0.4
4.0	37±2	19±1	3.0±0.25	11.7±1	12.7±1.0	25.5±2	8.8±0.4	15.7±0.7	3.9±0.4
4.2	37±2	18.5±1	3.15±0.25	10.2±0.8	13.0±1.0	25.5±2	8.5±0.4	15.2±0.7	3.9±0.4
4.4	37±2	18.5±1	3.15±0.25	9.8±0.8	13.0±1.0	24.5±1.5	8.4±0.4	15.2±0.7	3.8±0.4
4.6	36.5±2	18±1	3.15±0.25	9.3±0.7	12.8±1.0	24.0±1.5	8.4±0.4	15.0±0.7	3.8±0.4
4.8	35±2	17.5±1	3.15±0.25	8.6±0.7	12.7±1.0	23.5±1.5	8.4±0.4	15.0±0.7	3.75±0.3

TABLE III. - Concluded. MEASURED ABSOLUTE NEUTRON LEAKAGE SPECTRA AT 2 METERS FROM SPHERES CONTAINING Am-Be SOURCE

Energy, MeV	Bare source	Beryllium	Polyethylene (CH_2)	Lead	Niobium	Molybdenum	Tantalum	Tungsten	
								Small	Large
	Absolute neutron spectra, neutrons/cm^2-sec-MeV								
5.0	34.5±2	16.5±1	3.05±0.2	7.8±0.7	11.5±1.0	22.5±1.5	8.5±0.4	14.5±0.7	3.50±0.3
5.2	33±2	15±1	2.80±0.2	7.2±0.7	11.0±0.8	21.5±1.5	7.7±0.4	13.5±0.6	3.30±0.3
5.4	31.5±2	13.7±1	2.60±0.2	6.7±0.6	10.0±0.8	21.0±1.5	7.4±0.4	12.5±0.6	3.10±0.3
5.6	29±2	12.6±0.8	2.50±0.2	6.3±0.6	9.5±0.7	19.5±1.5	6.8±0.3	11.6±0.6	2.90±0.3
5.8	27.5±2	12.0±0.6	2.40±0.15	6.0±0.5	9.0±0.6	19.0±1.5	6.4±0.3	11.0±0.6	2.90±0.3
6.0	25±2	11.1±0.6	2.35±0.15	5.5±0.5	8.5±0.5	17.0±1.5	5.9±0.3	10.0±0.6	2.65±0.2
6.2	23.5±2	10.5±0.5	2.25±0.15	5.0±0.4	7.7±0.5	16.0±1	5.5±0.3	9.0±0.5	2.50±0.2
6.4	20.5±2	9.5±0.5	2.20±0.15	4.8±0.4	6.8±0.5	14.0±1	5.0±0.3	8.0±0.5	2.30±0.2
6.6	19.5±1.5	8.7±0.5	2.15±0.15	4.6±0.4	6.4±0.4	12.5±1	4.5±0.3	7.2±0.4	2.15±0.15
6.8	18±1.5	8.5±0.5	2.05±0.10	4.2±0.3	6.2±0.4	12.0±1	4.1±0.2	6.9±0.4	2.00±0.15
7.0	18±1.5	8.0±0.5	1.90±0.10	4.0±0.3	5.8±0.4	11.7±1	3.9±0.2	6.9±0.4	1.85±0.15
7.2	17.5±1	7.7±0.5	1.85±0.10	3.9±0.3	5.7±0.4	11.7±1	3.9±0.2	6.6±0.3	1.80±0.15
7.4	17.2±1	7.4±0.5	1.65±0.10	3.7±0.25	5.5±0.4	11.4±1	3.5±0.2	6.5±0.3	1.75±0.15
7.6	16.5±1	7.0±0.4	1.52±0.08	3.6±0.25	5.3±0.4	11.1±1	3.4±0.2	6.5±0.3	1.75±0.15
7.8	16.0±1	6.6±0.4	1.40±0.08	3.4±0.25	5.0±0.3	10.7±0.8	3.4±0.2	6.1±0.3	1.70±0.15
8.0	15.5±1	6.6±0.4	1.30±0.08	3.0±0.2	4.8±0.3	10.2±0.8	3.6±0.2	5.8±0.3	1.65±0.15
8.2	14.2±1	6.1±0.4	1.20±0.07	2.75±0.2	4.6±0.3	9.4±0.7	3.3±0.2	5.3±0.3	1.60±0.1
8.4	13.7±1	5.3±0.3	1.09±0.07	2.35±0.15	4.0±0.3	8.4±0.6	2.9±0.2	4.6±0.3	1.40±0.1
8.6	11.5±0.8	4.6±0.3	.98±0.07	2.15±0.15	3.5±0.3	7.3±0.6	2.55±0.15	3.9±0.3	1.20±0.1
8.8	9.2±0.8	3.8±0.3	.90±0.07	1.90±0.15	2.9±0.3	6.5±0.6	2.2±0.15	3.35±0.2	.97±0.09
9.0	7.7±0.7	3.35±0.3	.84±0.07	1.75±0.15	2.65±0.2	5.2±0.4	2.0±0.15	3.0±0.2	.87±0.08
9.2	6.8±0.5	2.90±0.25	.80±0.07	1.56±0.10	2.40±0.2	4.7±0.4	1.80±0.1	2.7±0.2	.77±0.08
9.4	6.5±0.4	2.75±0.25	.78±0.07	1.45±0.10	2.30±0.2	4.6±0.3	1.65±0.1	2.5±0.2	.73±0.07
9.6	6.4±0.4	2.62±0.24	.73±0.06	1.35±0.10	2.25±0.2	4.4±0.3	1.65±0.1	2.5±0.2	.68±0.07
9.8	6.2±0.3	2.35±0.2	.68±0.06	1.25±0.10	2.05±0.2	4.0±0.3	1.55±0.1	2.4±0.2	.65±0.06
10.0	5.8±0.3	2.20±0.2	.60±0.05	1.15±0.10	1.85±0.15	3.6±0.3	1.5±0.1	2.2±0.2	.63±0.06
10.2	5.2±0.3	2.05±0.15	.50±0.04	.92±0.09	1.50±0.10	3.2±0.3	1.4±0.1	2.05±0.15	.56±0.06
10.4	4.2±0.3	1.65±0.15	.40±0.04	.75±0.07	1.27±0.10	2.9±0.3	1.3±0.1	1.85±0.15	.48±0.05
10.6	3.4±0.3	1.35±0.15	.31±0.03	.58±0.07	.92±0.08	2.2±0.3	1.0±0.1	1.45±0.10	.39±0.05
10.8	2.5±0.3	1.00±0.25	.25±0.025	.42±0.06	.73±0.07	1.7±0.2	----------	1.10±0.08	.34±0.05
11.0	1.7±0.2	----------	.165±0.02	.32±0.05	.55±0.05	1.6±0.25	----------	----------	.26±0.05
11.2	1.2±0.2	----------	.125±0.015	.21±0.04	.39±0.05	----------	----------	----------	.18±0.05
11.4	--------	----------	----------	.10±0.02	.28±0.05	----------	----------	----------	.11±0.05
11.6	--------	----------	----------	----------	.21±0.05	----------	----------	----------	----------
11.8	--------	----------	----------	----------	.16±0.05	----------	----------	----------	----------
12.0	--------	----------	----------	----------	.11±0.05	----------	----------	----------	----------

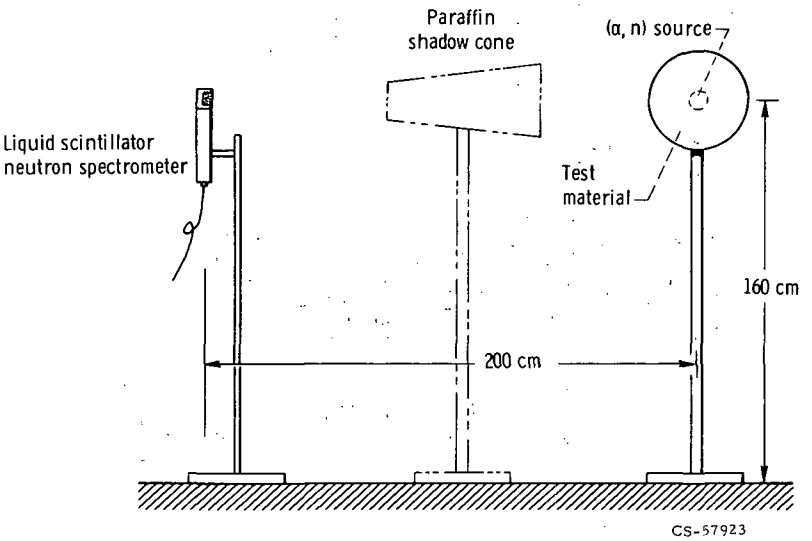

Figure 1. - Experimental arrangement for neutron leakage spectra measurements from spheres of test material containing an americium-beryllium (α, n) source.

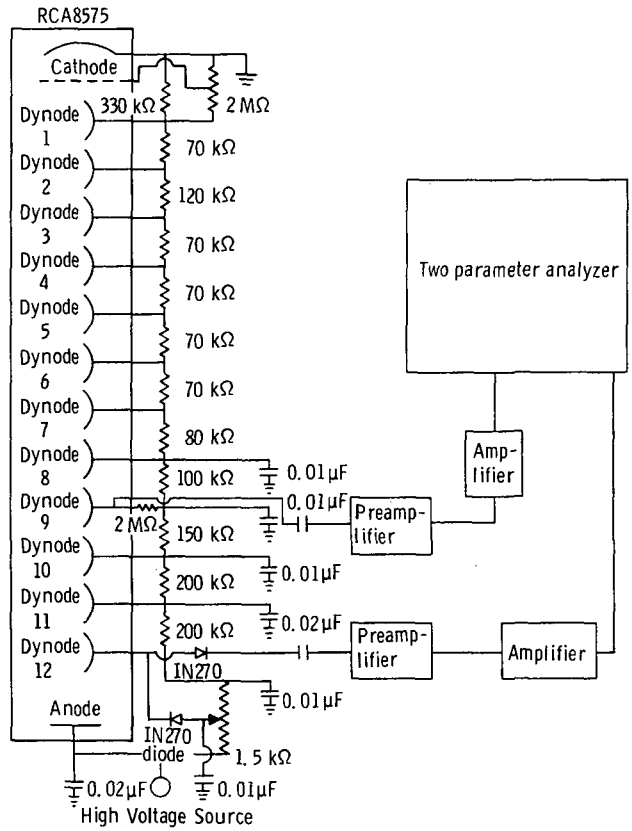

Figure 2. - Spectrometer block diagram and photomultiplier tube base circuit.

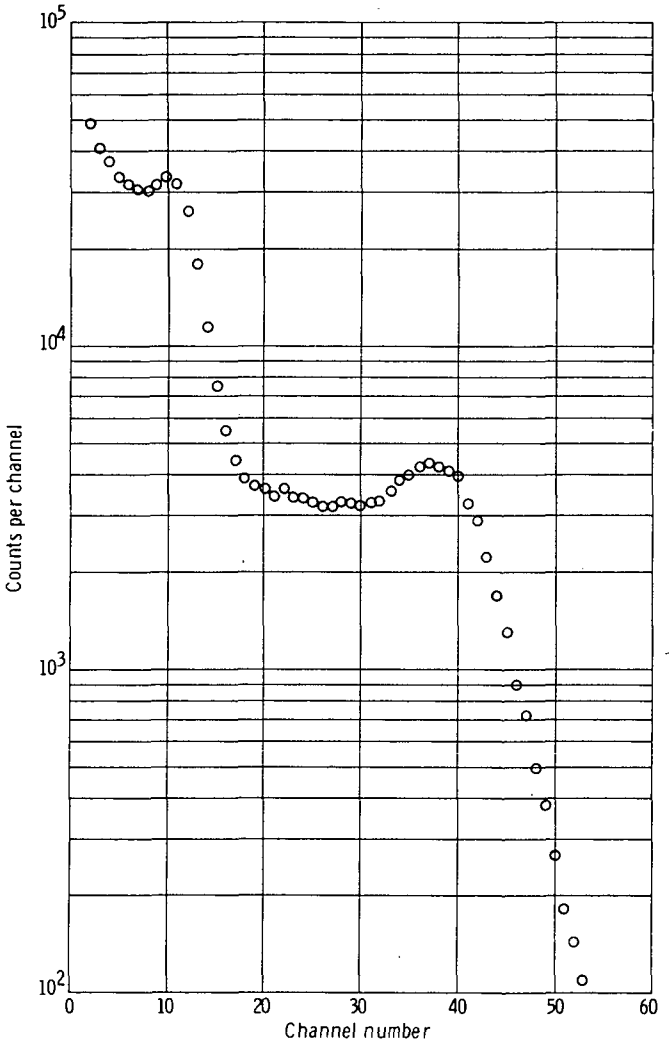

Figure 3. - Sodium-22 calibration for 5 by 5 centimeter NE 213 liquid scintillator.

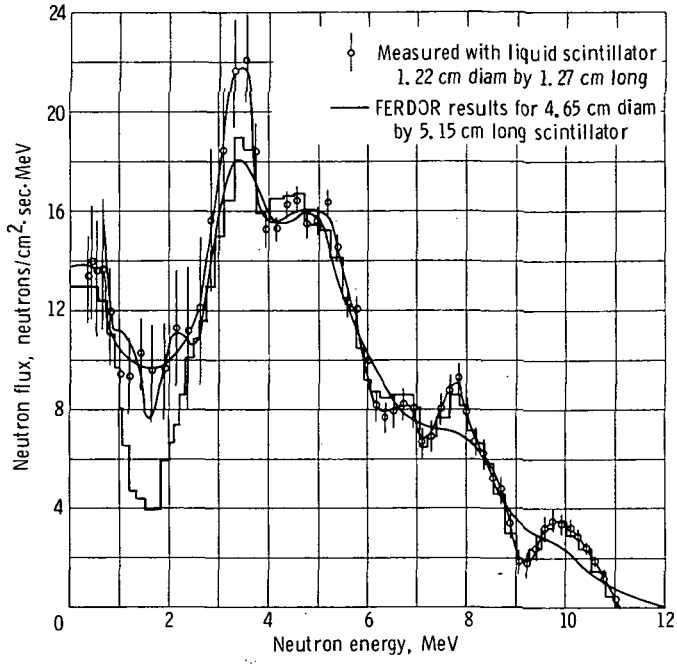

Figure 4. - Small polonium-beryllium neutron source spectrum. Histogram represents virgin (α, n) source spectrum.

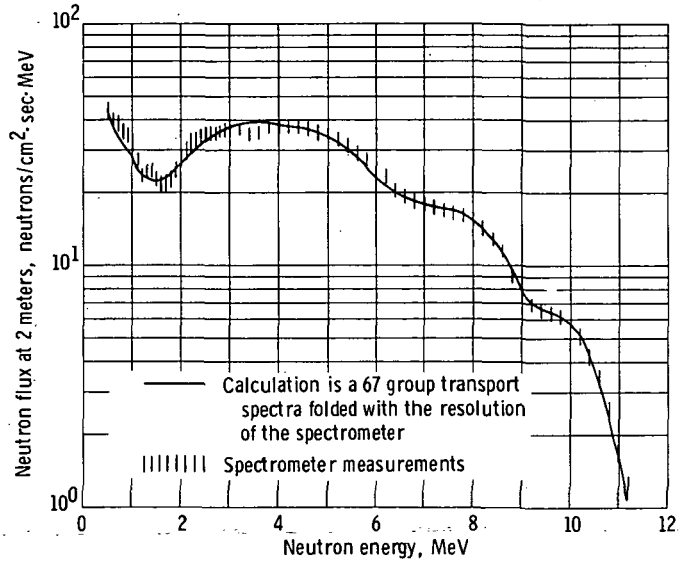

Figure 5. - Comparison of measured and calculated neutron leakage flux spectra at 2 meters from bare americium-beryllium source in air.

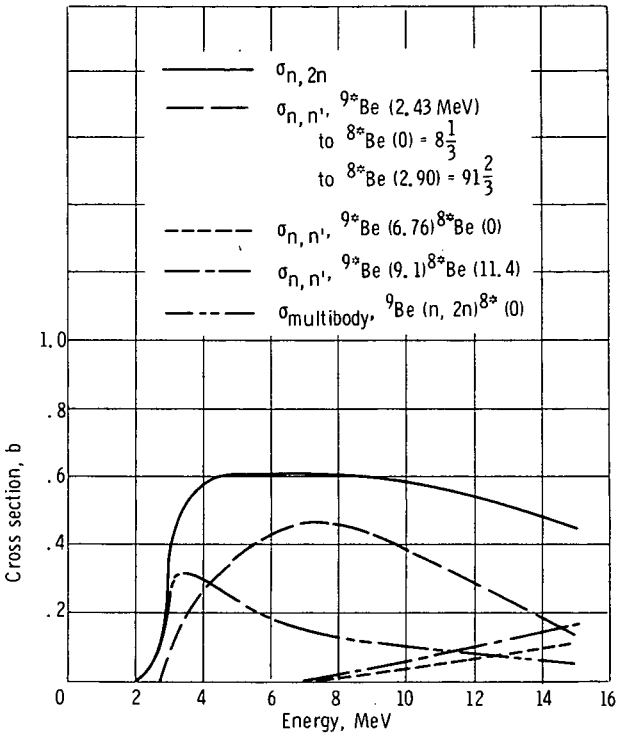

Figure 6. - Cross sections for decay modes of Be(n, 2n) reaction; evaluated by Perkins (ref. 38).

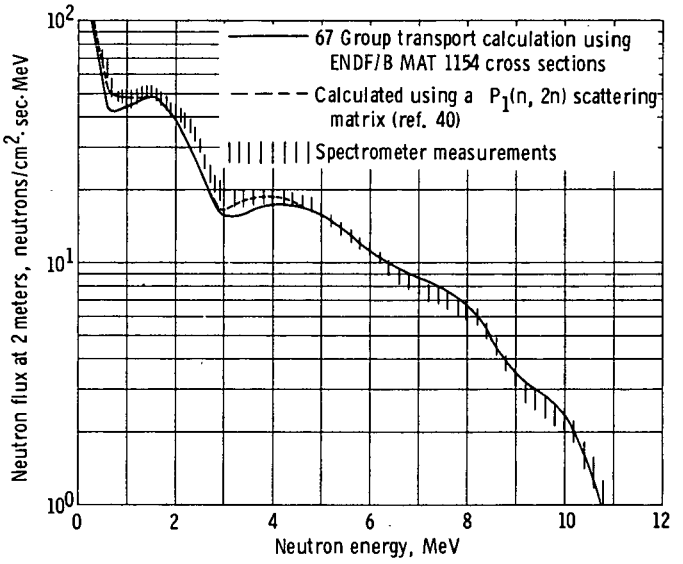

Figure 7. - Neutron leakage spectra for americium-beryllium source in beryllium sphere.

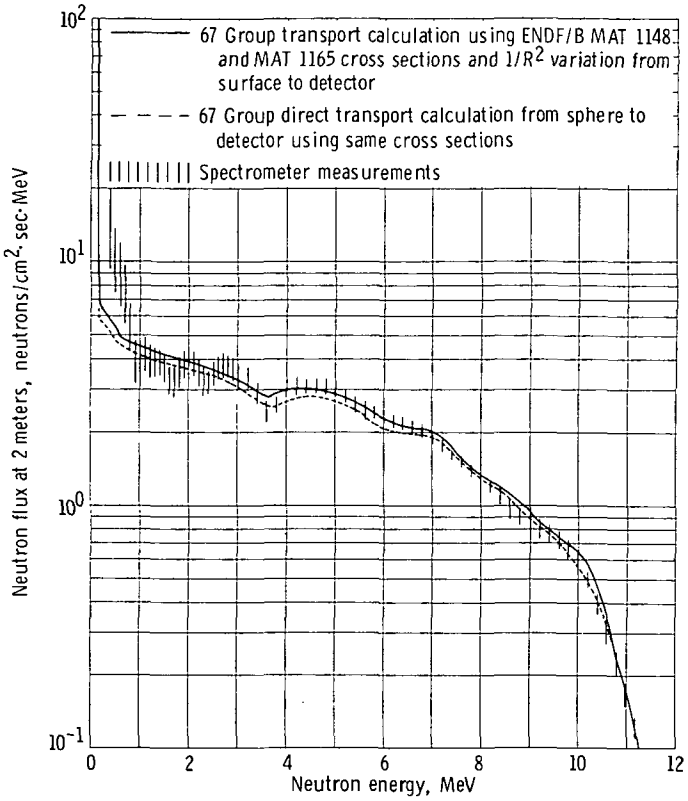

Figure 8. - Neutron leakage spectra for americium-beryllium source in polyethylene sphere.

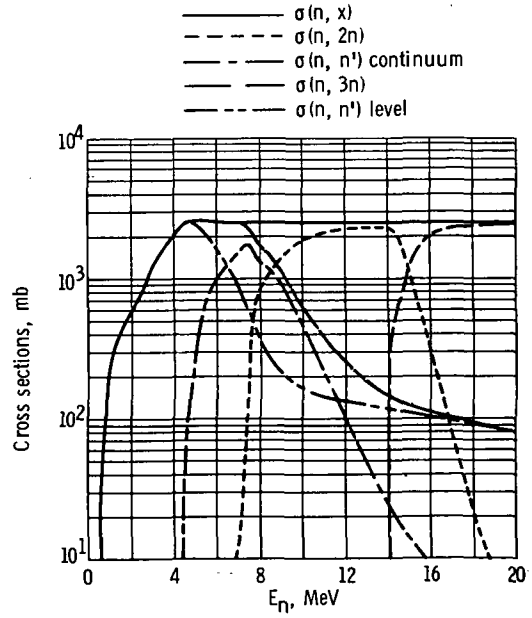

Figure 9. - Evaluated natural lead nonelastic cross sections and their various components (from ref. 41.) Natural lead, 53% ^{208}Pb, 23% ^{207}Pb, 24% ^{206}Pb.

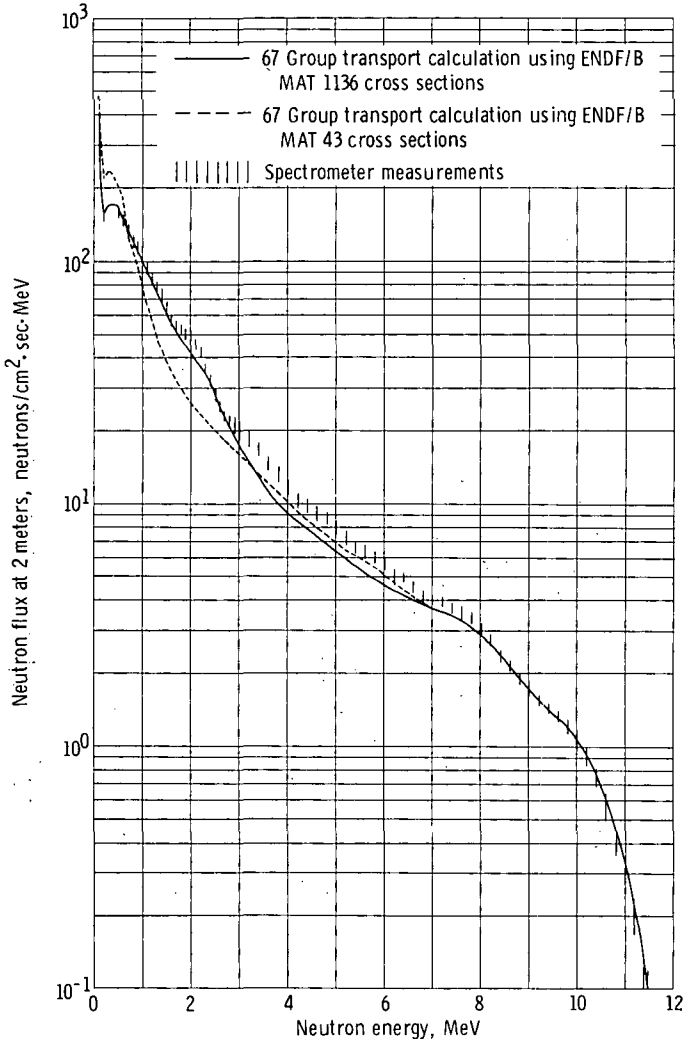

Figure 10. - Neutron leakage spectra for americium-beryllium source in natural lead sphere.

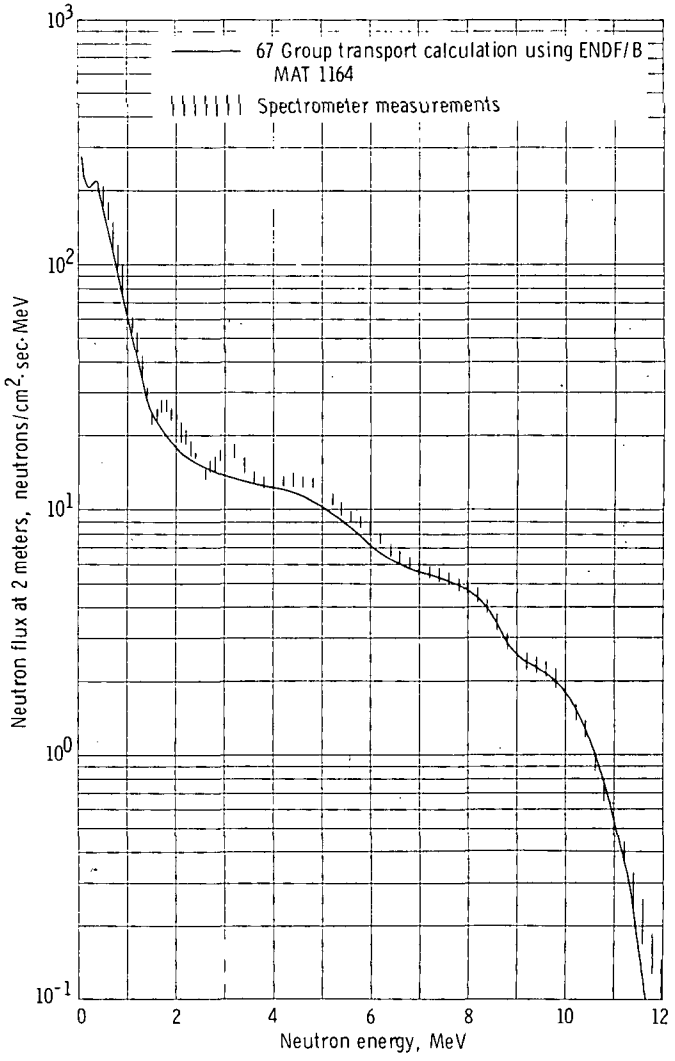

Figure 11. - Neutron leakage spectra for americium-beryllium source in niobium sphere.

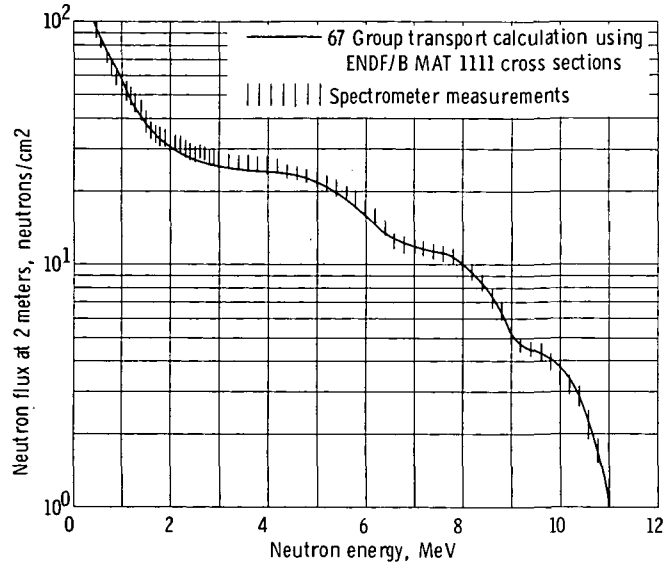

Figure 12. - Neutron leakage spectra for americium-beryllium source in molybdenum sphere.

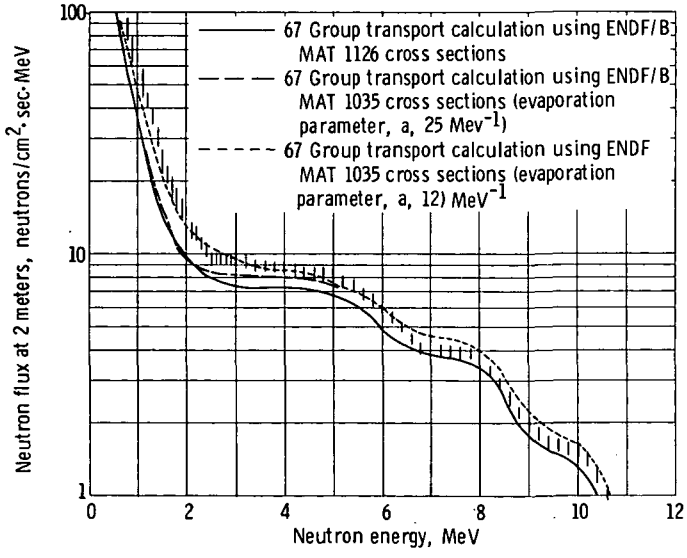

Figure 13. - Neutron leakage spectra for americium-beryllium source in tantalum sphere.

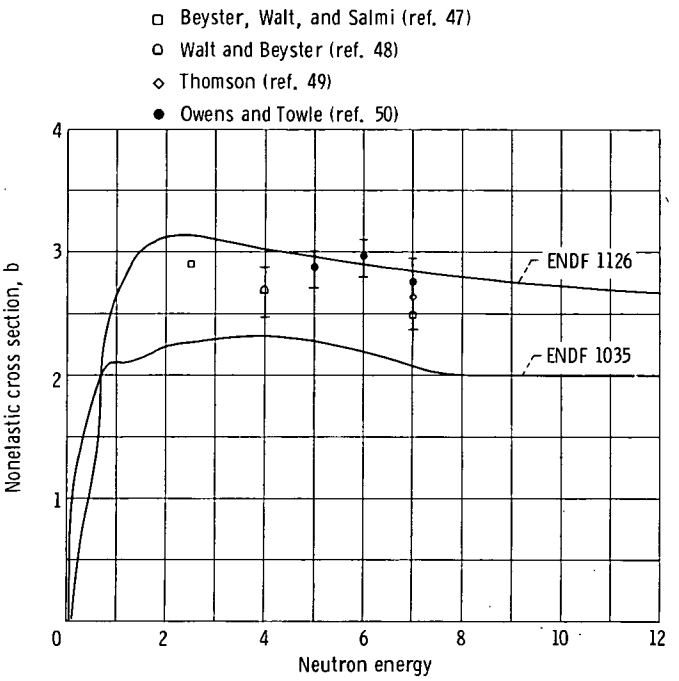

Figure 14. - Evaluated total nonelastic cross sections for tantalum.

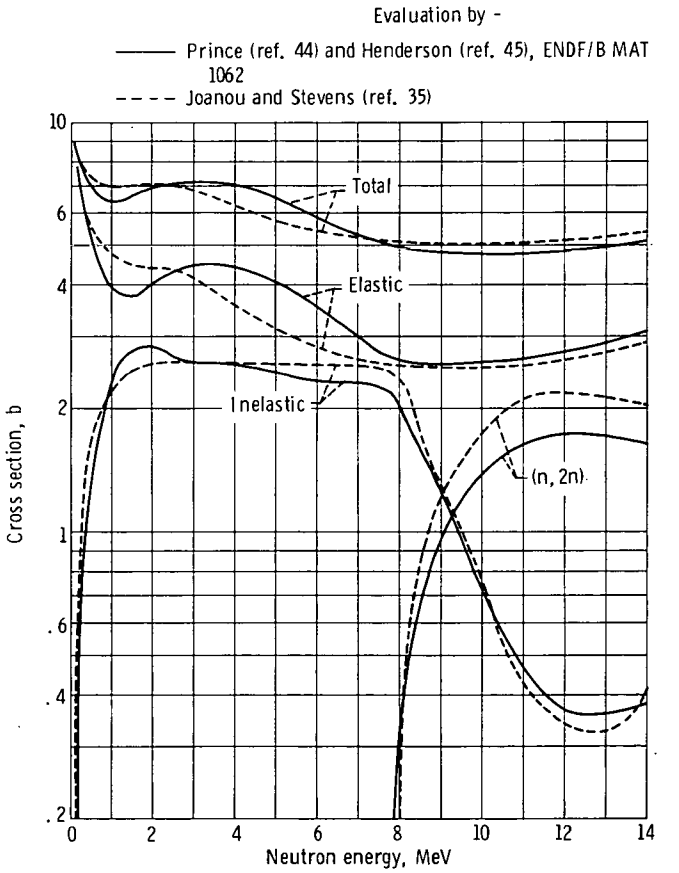

Figure 15. - Evaluated high energy cross sections for tungsten-184.

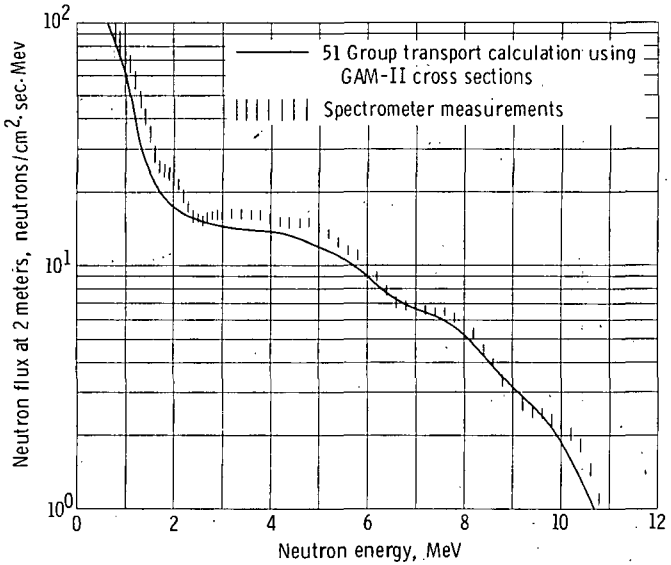

Figure 16. - Neutron leakage spectrum for americium-beryllium source in small tungsten sphere.

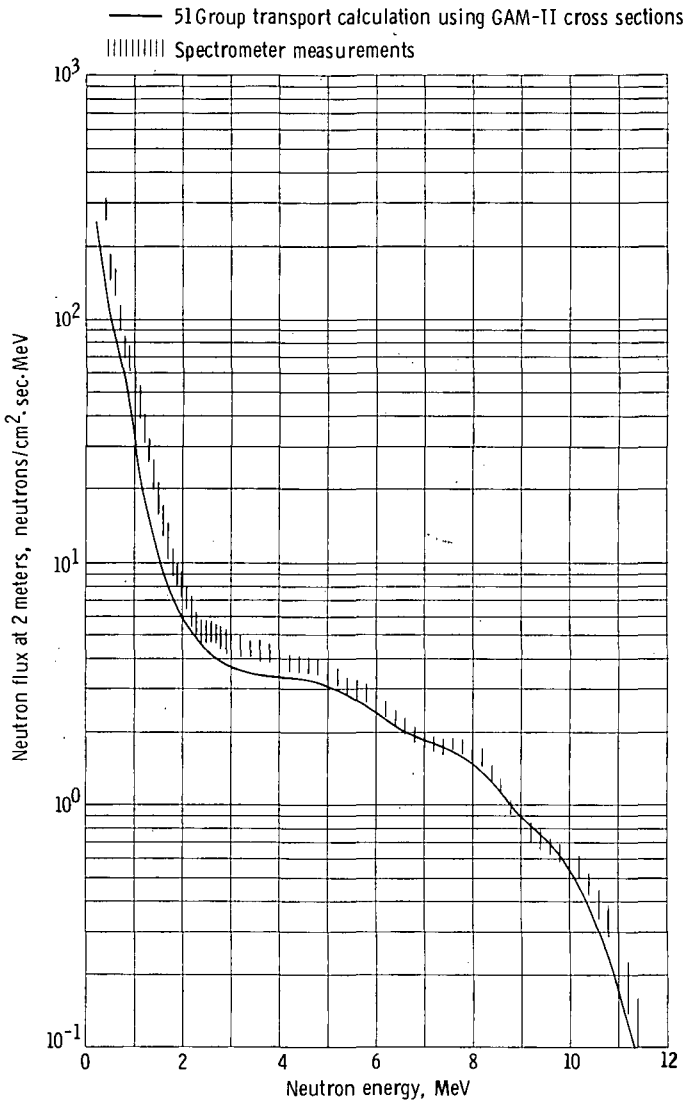

Figure 17. - Neutron leakage spectrum for americium-beryllium source in large tungsten sphere.

NATIONAL AERONAUTICS AND SPACE ADMINISTRATION
WASHINGTON, D.C. 20546

OFFICIAL BUSINESS
PENALTY FOR PRIVATE USE $300

SPECIAL FOURTH-CLASS RATE BOOK

POSTAGE AND FEES PAID
NATIONAL AERONAUTICS AND SPACE ADMINISTRATION
451

U.S.MAIL

POSTMASTER: If Undeliverable (Section 158 Postal Manual) Do Not Return

"The aeronautical and space activities of the United States shall be conducted so as to contribute . . . to the expansion of human knowledge of phenomena in the atmosphere and space. The Administration shall provide for the widest practicable and appropriate dissemination of information concerning its activities and the results thereof."

—NATIONAL AERONAUTICS AND SPACE ACT OF 1958

NASA SCIENTIFIC AND TECHNICAL PUBLICATIONS

TECHNICAL REPORTS: Scientific and technical information considered important, complete, and a lasting contribution to existing knowledge.

TECHNICAL NOTES: Information less broad in scope but nevertheless of importance as a contribution to existing knowledge.

TECHNICAL MEMORANDUMS: Information receiving limited distribution because of preliminary data, security classification, or other reasons. Also includes conference proceedings with either limited or unlimited distribution.

CONTRACTOR REPORTS: Scientific and technical information generated under a NASA contract or grant and considered an important contribution to existing knowledge.

TECHNICAL TRANSLATIONS: Information published in a foreign language considered to merit NASA distribution in English.

SPECIAL PUBLICATIONS: Information derived from or of value to NASA activities. Publications include final reports of major projects, monographs, data compilations, handbooks, sourcebooks, and special bibliographies.

TECHNOLOGY UTILIZATION PUBLICATIONS: Information on technology used by NASA that may be of particular interest in commercial and other non-aerospace applications. Publications include Tech Briefs, Technology Utilization Reports and Technology Surveys.

Details on the availability of these publications may be obtained from:

SCIENTIFIC AND TECHNICAL INFORMATION OFFICE

NATIONAL AERONAUTICS AND SPACE ADMINISTRATION

Washington, D.C. 20546